Tampere University

Faheem Ahmed Bhatti

NEW PHOSPHATE BIOACTIVE GLASSES WITH ENHANCED THERMAL PROPERTIES FOR 3D SCAFFOLD PROCESSING USING ROBOCASTING

The Faculty of Medicine and
Health Technology
Master of Science Thesis
November 2019

ABSTRACT

Faheem Ahmed Bhatti: New Phosphate Bioactive Glasses With Enhanced Thermal Properties For 3D Scaffold Processing Using Robocasting.
Master of Science Thesis
Tampere University
Master of Science in Electrical Engineering
November 2019

Phosphate bioactive glasses are the potential substitutes of typical silicate bioactive glasses for repair and regeneration of the defected bone due to their resemblance to the natural bone. In earlier studies, thermal, bioactive and structural properties of different phosphate bioactive glasses were investigated by introducing various elements. Furthermore, in some studies these glasses were utilized in scaffolds fabrication using methods like powder technique and foaming technique. But these techniques produced scaffolds with reduced mechanical properties due to large pores size.

In this thesis, new phosphate bioactive glasses with compositions; $45P_2O_5$, $2.5B_2O_3$, $2.5SiO_2$, $10Na_2O$, 20CaO, (20-x)SrO, xMgO in mol% (x = 0, 5 ,10, 15 and 20) were prepared with two particle sizes i.e. <38µm and 125-250µm. The aim was to develop phosphate bioactive glasses that can be sintered without losing their bioactivity. Thermal analysis was performed for these glasses in which glass transition and crystallization temperatures were increased with increasing amount of MgO. By further increasing the MgO content from 15 and 20 mol%, crystallization peaks disappeared. Bioactivity studies were performed in Simulated Body Fluid (SBF) at 37°C. The ion release profile was highly function of the particles size, as can be expected from glasses. A rapid ion release, within 1 day was seen for the smaller particle size. Larger particle size, 125-250µm, released ions continuously for 2 weeks. FTIR of the glass structure revealed two new bands after 2 weeks time point, especially in the sample substituted with 20 mol% of MgO for SrO, that indicated CaP layer formation.

Based on thermal and bioactive properties, suitable glass compositions were chosen i.e. x = 10 and 15. These compositions were subjected to scaffold fabrication using robocasting technique in which printing head movement was controlled by programmed printing script. Ink, prepared from glass powders and Pluronic F-127 binder, was extruded to get three-dimensional scaffolds and then further sintered to obtained mechanically stable, amorphous, scaffolds. *In-vitro* dissolution revealed the formation of CaP layer faster and prominent in x = 15 glass scaffold. Furthermore, mechanical strength of both compositional scaffolds remained in the range of cancellous bone compressive strength even after two weeks of immersion in SBF.

Keywords: phosphate bioactive glass, scaffold, robocasting, bone tissue engineering, crystallization, sintering

PREFACE

This thesis study was conducted in Bioceramics, bioglass and biocomposites research group at Tampere University Hervanta Campus. I wholeheartedly express my gratitude to Assoc. Prof. Jonathan Massera for providing me an opportunity to work on this fascinating thesis topic under his tireless and expert supervision. I also would like to thank Ayush, Sanna, Henriikka and Mari, without whose cooperation it would be difficult to perform my laboratory experiments.

Finally, I would like to thank my family for their blessings and friends for their support during the journey of my master thesis work.

Tampere, 4th November 2019

Faheem Ahmed Bhatti

CONTENTS

LIST OF FIGURES

LIST OF TABLES

LIST OF SYMBOLS AND ABBREVIATIONS

TE	Tissue Engineering
RM	Regenerative medicine
BTE	Bone Tissue Engineering
BO	Bridging Oxygen
NBO	Non-Bridging Oxygen
RT	Room Temperature
SBF	Simulated Body Fluid
HA	Hydroxyapatite
CPCs	Calcium Phosphate Ceramics
SD	Standard Deviation
AM	Additive Manufacturing
SFF	Solid Free Form Fabrication
SL	Stereolithography
RP	Rapid Prototyping
SLS	Selective Laser Sintering
DTA	Differential Thermal Analysis
ICP-OES	Inductive Coupled Plasma – Optical Emission Spectroscopy
FTIR-ATR	Fourier Transform Infrared Spectroscopy
XRD	X-Ray Diffraction
ACP	Amorphous Calcium Phosphate
T_g	Glass Transition Temperature
T_x	Onset of Crystallization
T_p	Peak Crystallization Temperature
ΔT	Hot Working Window
MPa	Megapascal

1. INTRODUCTION

Any damage to the tissue caused by disease, trauma, aging or tumor removal requires repair and regeneration (Sharif, et al., 2016). When considering bone regeneration, autograft (bone harvested from the patients own body), allograft (graft taken from someone else body) and xenograft (graft taken from another species) are used in current treatments. Autograft has been a gold standard for bone replacing for many years. The bone is mainly harvested from the iliac crest. Despite being the gold standard, limitations such as limited availability, donor site morbidity and chance of infections are drawbacks that must be pointed out. Allograft transplantation may cause pathogen transfers, immune rejections and risk of infections in recipients' body. Xenograft is cheap and readily available but has limitations like ethical issue and chronic rejections (Salgado, et al., 2004; Al-Qaysi, 2018). To overcome the limitations of these grafts, biomaterials are being investigated such as polymers, metals, ceramics and composites. Among these materials, ceramics have gained importance due to their bioactive property i.e., they elicit a biological response leading to bond formation between tissue and material. (Ratner, et al., 1996). Examples of ceramics are calcium phosphate ceramics (CPCs) that are tunable and have been utilized for bone repair and augmentation. Their surface properties allow the osteoblast adhesion and new bone stimulation. Most common CPCs are hydroxyapatite and tricalcium phosphate (Dorozhkin & Epple, 2002). Drawbacks of CPCs include poor mechanical properties which limits their use in non-load bearing applications, brittleness of the CPCs block which resists in filling bone defect perfectly (Yuan & Groot, 2005). These limitations gave rise to the research on bioactive glasses.

In 1969, the first bioactive glass named Bioglass® 45S5 (a silicate glass) developed by Professor Larry Hench, exhibited high bioactivity and had the ability to bond to soft and hard tissues. His discovery led to the extensive research in the field of bioactive glasses (Jones, 2013; Moya, et al., 1999). Bioglass® had two main features i.e., to inhibit foreign body reaction, and to form hydroxyapatite (HA) layer, that resembles the main mineral phase of the bone, upon immersion in aqueous solution, thus allowing bone healing (Hench, et al., 1971). However, thermal processing methods are not suitable for such silicate glasses due to induction of extensive crystallization during the process which is undesirable for bioactivity and also resist the proper sintering. (Filho, et al., 1996; Massera, et al., 2012). Furthermore, the dissolution of silicate glasses has been well

studied and is nowadays well understood (Sepulveda, et al., 2002). The incongruent dissolution mechanism of silicate bioactive glasses led to the remnants of silicate bioactive glass after 14 years of operation (Lindfors, et al., 2010). These short comings of silicate glasses didn't make a breakthrough in the clinic which led to the research on the different substitutes such as borate and phosphate glasses.

Phosphate bioactive glasses due to their resemblance to the natural bone, are highly attractive as a biomaterial. However, simple phosphate glasses degrade fast and, thus, have a low chemical durability. These glasses can be used as a bioresorbable materials in applications such as: suture thread and bone fracture fixation (Ahmed, et al., 2004a). Phosphate glasses are made bioactive by tailoring their composition, this way, the rate of degradation can be controlled and become suitable for use in bone repair and reconstruction (Bunker, et al., 1984; Clement, et al., 1999). Furthermore, phosphate bioactive glasses have good thermal properties and, thus, provide large processing window, as evidenced in previous studies on bioactive phosphate fibers (Ahmed, et al., 2004b; Massera, et al., 2015). Phosphate bioactive glass family have also been researched, lately, by doping with various elements i.e. Ag, Cu and Fe to assess their effect on properties such as thermal processability, in-vitro dissolution properties and structural properties (Mishra, et al., 2016; Mishra, et al., 2017; Lopez-Iscoa, et al., 2019).

Scaffolds, which are porous 3D construct, act as a temporary template in the body. Scaffold degrades after natural healing of the tissues. Selection of the scaffold materials are based on future applications (structural support or drug delivery) (Sultana, 2013; Jones, 2013; Fu, et al., 2011; Khan, et al., 2008). Mostly, bioactive glasses are considered as attractive materials for scaffold development due to ease in controlling their chemical composition and, thus, degradation rate (Fu, et al., 2011). Scaffolds of phosphate based bioactive glasses have been fabricated using techniques such as powder technology and foaming technique (Ruiz-Aguilar, et al., 2019). However, production of scaffolds with large pores through these techniques results in poor mechanical strength of the scaffolds (Erasmus, et al., 2018).

In this thesis project, the attempt is to produce new phosphate bioactive glasses with compositions that can be sintered and also show bioactivity. Five different compositions are developed in which MgO replaces SrO by increment of 5 mol% with the aim to study the effect of MgO addition on the thermal, structural and bioactive properties of phosphate bioactive glasses. MgO is known to increase the crystallization temperature when added in the glass composition (Islam, et al., 2017). Successful characterization of these glasses allowed to choose two best compositions that can be used to fabricate scaffolds using robocasting technique. Characterization of both glass compositions and scaffolds

include: differential thermal analysis (DTA) and X-Ray diffraction (XRD) to reveal thermal properties, *in-vitro* dissolution test to examine the bioactivity of the glasses, fourier transform infrared spectroscopy (FTIR) to evaluate structural change of the glass surface and, finally, compression test of fabricated scaffolds to observe mechanical strength. Successful results from these analyses pave the way for these phosphate glasses to application in bone tissue engineering applications.

This thesis comprises of theoretical background (chapter 2) in which key concepts related to this thesis are given, materials and methods (chapter 3) where experimental work done in this thesis is explained, results and discussion (chapter 4) in which obtained results are mentioned and discussed. Finally, conclusion and key findings of the thesis project are presented in chapter 5.

2. THEORATICAL BACKGROUND

2.1 Bone tissue engineering

Current clinical treatments for bone defects have some limitations and complications such as donor site morbidity, immune rejection, shortage of bone grafts and pathogens transfer. Bone tissue engineering is a relatively new field which focuses on alternative treatment options that could ideally suppress these issues in a reliable, affordable and physiologically acceptable manner (Sultana, 2013; Amini, et al., 2012).

2.1.1 Bone

The human skeleton is made up of approximately 206 bones which are distributed in axial skeleton that contains skull, sternum, vertebrae, ribs and hyoid and the peripheral skeleton that includes limps and pelvis bones. All together their function is to provide mechanical strength, maintain structure and shape of the body, protect organs from external damage, help in locomotion of the body and act as a reservoir for the cytokines and growth factors. Bones in their life-time constantly model to adapt the biomechanical forces and remodel to keep themselves strong by replacing old and weak bones with new and mechanically stronger bones. (Kardamakis, et al., 2009, p. 4; Clarke, 2008).

According to anatomy, a human bone has three components including periosteum, the cortex and the medulla. Periosteum separates the bone from soft tissues due to its presence at the outer surface of the bone and also maintain the shape and size of the bone. It has two layers i.e. inner cellular layer and outer fibrous layer. Inner layer contains cells such as osteoprogenitor, fibroblasts and osteoblasts along with sympathetic nerves and microvessels. Outer layer contains fibroblasts cells, collagen, elastin fibers along with a network of blood vessels and nerves. Inner layer reduces its cellularity with age. The cortex is a thick part of the bone that is present below the periosteum. It is made up of compact bone. Due to its hardness, it is in great proportion in long bones which also handles the mechanical forces. Last component, medulla of the bone is comprised of cancellous bone which is spongy in shape and its percentage is more in bones of vertebral column (Kardamakis, et al., 2009).

Bone cells, despite contributing for less than 2% to the bone mass formation, play an important role in bones functionality. They are of four types: osteoblasts, osteocytes, osteogenic cells, and osteoclasts (Figure 1). Osteoblasts are present in the growing part of the bone and are responsible for mineralizing and making new bones. Osteoblasts

secrete collagen especially type-1 and other proteins which help in bone formation. Eventually they get trapped in collagen matrix and turn into osteocytes. Osteocytes are the most common types and primary cells of the mature bone. Its function is to regulate the mineral concentration in the matrix by secreting enzymes. Osteoblasts and osteocytes lack the ability to divide, therefore, they are osteogenic cells also called osteoprogenitor cells which differentiate into osteoblasts when the old ones die. They are the only bone cells which divide and are present in the periosteum and the endosteum cellular layer. Last cell type are osteoclasts, produced by macrophages and monocytes and are multinucleated, resorb unnecessary and injured bones to release minerals from the bone tissue (Biga, et al., 2019). Improper function of osteoclasts can lead to several bone diseases, including Paget disease (formation of disorganized bone tissue), osteoporosis (non-compensable bone resorption) and osteopetrosis (bone becomes hard due to less resorption of bone by osteoclasts) (Kardamakis, et al., 2009).

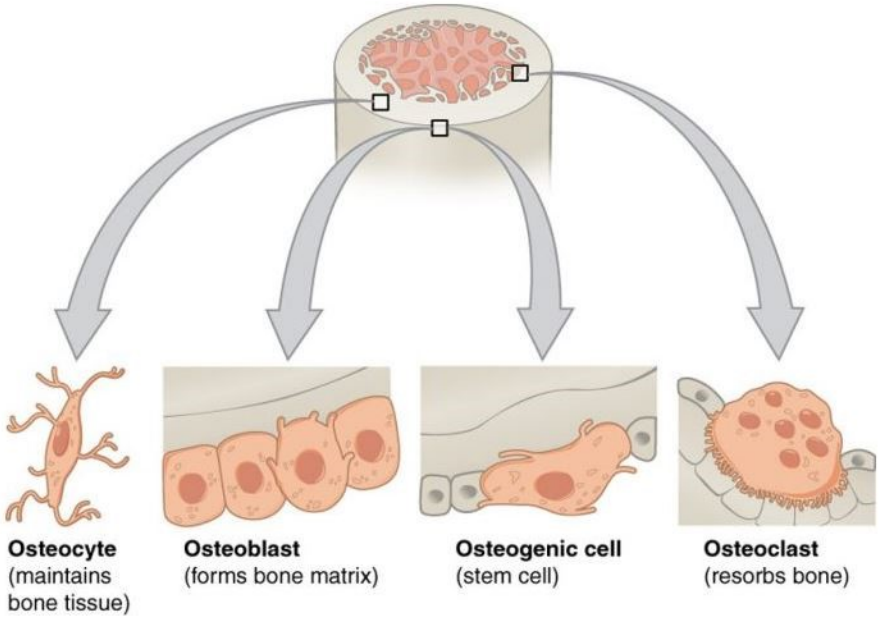

Figure 1. *Bone cell types and their positions (Biga, et al., 2019)*

The change in factors like person's age, gender, disease, bone deformation rate, its location and porosity highly affect the mechanical properties of the bone. It has been observed that moisture and mineralization have a great impact on bone rigidity. Table 1 shows the mechanical strength of a healthy human cancellous and cortical bone (Chittibabu, et al., 2016; Fu, et al., 2011).

Table 1. Mechanical properties of cancellous and cortical bones (Fu, et al., 2011).

Bones	Compressive strength (MPa)	Flexural strength (MPa)	Tensile strength (MPa)	Modulus (GPa)	Porosity (%)	Fracture toughness ($MPa \cdot m^{1/2}$)
Cancellous bone	2-12	10-20	1-5	0.1-5	0.1-0.8	50-90
Cortical bone	100-150	135-193	50-151	10-20	2-12	5-10

2.1.2 Allopathic medicine

Bone repair and regeneration is required when the tissue is damaged due to disease, aging, traumatic injuries or tumour removal. According to the report, in U.S, each year approximately 6.2 million bone fractures occur and about 10% do not recover properly. 10 million people are affected by osteoporosis and an increase by 4 million is expected by 2020, which is expected to lead to 25 billion dollars expenditure on healthcare annually. After blood, bone is believed to be the most transplanted tissues in the body. Every year around 2.2 million bone grafts are surgically implanted globally to aid bone healing (Fu, et al., 2011; Jones, 2013). It should be noted that bone repair reinstates the physiological structure of the bone whereas, bone regeneration is the process of forming new bone tissue (Al-Qaysi, 2018).

Bone grafting is one of the treatments used when the bone is fractured or part of it is absent. Common approaches for bone grafting are autografts, allografts and xenografts. Autograft can be extracted from patient´s own body and are osteoconductive, osteoinductive, and osteogenic. It is the gold standard approach in treating bone defects. However, it has limitations like extracted graft may not cover the large defect, donor site infection, morbidity, chronic pain after extraction and concerns about availability due to limited supply of the tissue (Sharif, et al., 2016; Edward, et al., 1996). Allograft is harvested from some other individual that, unlike autografts, can cover wider bone defects but the major drawbacks are disease transmission, evoking of immunological responses and high cost (Fu, et al., 2011; Sharif, et al., 2016). Deproteinated xenografts are extracted from bovine or pig to make inorganic bone scaffold. Their use in bone repair is limited because of personal, ethical and religious issues (Al-Qaysi, 2018).

Synthetic bioinert metals and polymers are also used in the treatment of defected tissues. Due to their inert behaviour they may cause severe inflammation as body does not accept them and as a result fibrous capsule is formed and surrounds the implant (Kress, et al., 2012). The bond between implant and fibrous capsule is typically weak which affects the implant performance that leads to repeated surgeries which consumes patient's

money and in return keeps the patient in discomfort (Jones, 2013; Nair & Laurencin, 2007).

2.1.3 Tissue engineering approach

Tissue engineering (TE) combines the methods and principles of engineering and life sciences to understand the relationship between healthy and diseased living tissue in order to develop the biological substitutes that restore the normal function of the body. TE has overcome the limitations of conventional treatments by introducing constructs and 3 dimensional porous scaffolds. Scaffolds, which mimic the properties and structure of the tissue are used in TE. They are typically fabricated according to the desired shape and size. Cells are embedded in scaffold with signaling molecules if needed which, later on, are cultured in a bioreactor before they are implanted in the patient. Implanted scaffold act as a temporary substrate and provide necessary support to the cells (Sultana, 2013).

Bone Tissue Engineering (BTE) is an emerging field that helps in regenerating bone tissues and restoring the functions with the help of osteoconductive scaffolds, osteogenic progenitor cells and osteoinductive growth factors (Sultana, 2013). BTE understands the biology and mechanics of the bone so that it can regenerate the new functional bone (Amini, et al., 2012). Scaffold is synthesized using biodegradable material which after temporary support degrades to stimulate the body's own healing mechanism and allow the natural healing of the bone (Jones, 2013).

Biological based approaches of BTE involve using cells and biomolecules to aid the repair and regeneration of the bone incorporated by biomaterials that give structure support and act as a platform for testing the viability of different biological parameters (Li, et al., 2017). As an example, hypertrophic cartilaginous constructs were obtained by growing rat nasal chondrocytes on a polyglycolic acid (PGA) scaffolds which were implanted into the rat cranial defect site. The process called analogous to endochondral ossification that resulted in angiogenesis, mineralization, and remodelling of the cartilage into bone (Bardsley, et al., 2017). Similarly, engineering-based approaches for BTE are mainly dependant on different techniques such as 3D printing and robocasting to produce ceramic bone graft substitutes with enhanced mechanical and structural properties that facilitates bone regeneration (Li, et al., 2017).

2.2 Synthetic biomaterials for TE

In regenerative medicine (RM), especially TE, biomaterials are the most important components of latest techniques that provide guidance and facilitate the behaviour and function of the cells. Latest techniques include cell therapies, where cells or matrices are delivered to the *in-vitro* constructed tissues by the carriers and in acellular therapies, where cells are stimulated by the materials to grow and differentiate from the healthy residual tissues in-situ. Materials used in such techniques provide three-dimensional support to control cell behaviour and guide the tissue formation and regeneration (Lutolf & Hubbell, 2005).

Tissues and organs have been reconstructed and regenerated using synthetic materials for about 100 years. Synthetic biomaterials should be biocompatible, biodegradable, have the mechanical, chemical and biological features such as eliciting an appropriate host response in order to be used in the body. The first ever implant materials were bioinert in nature and were used to support the mechanical function of the tissue. Later biomaterials were developed to be degradable and bioactive. In RM, variety of materials are used like metals, ceramics and polymers whose properties can be altered for use in different applications of TE like augmentation of existing tissues, new tissue growth promotion or replacement of the whole organ. Degradable materials are essential in the body where tissues need temporary support after which they heal themselves and allow the material to degrade eventually. Whereas, non-degradable implants have their own importance when it comes to replacing the damaged tissues function (Samavedi, et al., 2014).

Specifically, BTE requires materials that in addition to the properties above, also promote progenitor cells differentiation (Osteoinductive), facilitate native bone growth (Osteoconductive) and have the tendency to connect with the surrounding bone (Osteointegration property) (Stevens, 2008).

2.2.1 Ceramics

Ceramics used as biomaterials are usually called bioceramics. Generally, they are from synthetic or natural origin such as animal skeleton (hydroxyapatite or calcium carbonate) (Ben-Nissan, 2003). They are used as an alternative to metallic implants for repair and regeneration of defected parts of the body mostly in bone grafts and cements, dental implants, and orthopaedic load bearing coatings (hip acetabular cup) applications (Salinas & Regi, 2013). Biocompatibility, osteoconductivity, hard brittle surface, and corrosion resistance are the excellent properties found in bioceramics (Hasan, et al., 2013).

Ions, such as strontium, zinc, magnesium, manganese, and silicon release during resorption of bone grafts can affect positively on bone health and increases biocompatibility and mechanical properties of the implant. There are three types of bioceramics used in TE applications namely: Bioinert, bioactive, and bioresorbable bioceramics (Pina, et al., 2017).

Bioinert bioceramics include Alumina (Al_2O_3) and Zirconia (ZrO_2), which do not participate in biological activities due to their chemical inertness hence do not form bond with host tissues (Huang & S., 2014). They have high strength, hardness, cracking and corrosion resistance which make them suitable for applications in orthopaedics and dentistry (Figure 2). Alumina ceramics alone doesn't have sufficient fracture toughness therefore, zirconia is mixed with alumina to make zirconia-toughened alumina which not only increase toughness but also improve the wear properties. Zirconia based ceramics are well used in BTE due to its great mechanical properties: flexural strength above 1000 MPa and fracture toughness >8MPam$^{1/2}$ respectively (Pina, et al., 2017).

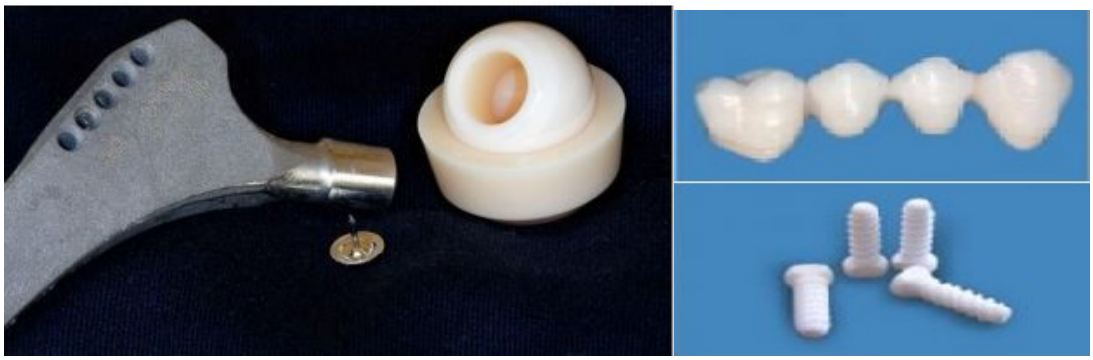

Figure 2. *Dental implants and hip joint prosthesis made of alumina and zirconia based ceramics (Pina, et al., 2017).*

Bioactive materials are the bioceramics that essentially facilitate the process of repair and regeneration of the bones when they are implanted in the body. Bioactive materials are famous because when they are introduced in the body, they get chemically bonded to the tissues (Kumar, et al., 2018; Bhushan, et al., 2015). Bioactive glasses and glass-ceramics are the examples of bioactive materials which are brittle and widely used in small bone damage filling and periodontal defects (Pina, et al., 2017). Whereas, biodegradable materials are completely degraded in the body after their specific time. Their chemical structure gets denatured by the body fluid and the chemicals released by them do not cause any toxic effects in-vivo. The biggest advantage of these materials is that

a patient doesn't need second surgery for their removal or adjustment. Calcium phosphate ceramics and HA are examples of biodegradable and bioactive bioceramics (Kumar, et al., 2018).

2.2.2 Polymers

Polymers in the form of natural and synthetic biomaterials, have been widely used in the TE and RM to fabricate scaffolds and also medical devices. Natural polymers are considered to be the first biodegradable materials used in clinical applications. They have the edge of possessing broad chemical, physical and bioactive properties that improve the cell performance in-vivo. Natural polymers that are used in TE are divided into two major classifications i.e., proteins and polysaccharides (Tang, et al., 2014; Dhandhayuthapani, et al., 2011).

Proteins are famous for degrading naturally in a controllable manner and are present in the natural tissue in a large amount. Because of their degradation properties, they are widely used as suturing material, drug delivery vehicles and scaffold materials etc. Proteins may include collagen, gelatin, elastin, silk, albumin, fibrin, keratin and chitosan. Whereas, polysaccharides are made up of many monosaccharides chains through glycoside bond or linkages. Chitosan, alginic acid, hyaluronic acid, cellulose and chondroitin sulfate are the polysaccharides used in different applications of TE. They are widely utilized in research due to their role in immune recognition and cell signalling (Tang, et al., 2014).

In general, guidance provided by synthetic biomaterials are useful in restoring the structure and function of damaged tissues. Similarly, synthetic polymers are preferred to be used in TE applications because their properties can be altered according to the requirements. They can be manufactured in large amount and in controlled condition and also possess long shelf time. Synthetic polymers possess good mechanical and physical properties (elastic modulus, tensile strength and degradation rate). Examples of synthetic polymers are PLA, PGA and its copolymer like PLGA which are mostly used in TE (Dhandhayuthapani, et al., 2011; Gunatillake, et al., 2006). Drawback is that the synthetic biodegradable polymers like PGA and PLLA exhibit inadequate degradation time when used as a scaffold. PGA and its copolymer PLLA reduce its tensile strength to 50% and resorb fast on the other hand, PLLA takes too much time to degrade when used in Scaffold material (Ikada, 2006). In general, polymers are not stronger than ceramics therefore ceramics are preferred over polymers for load-bearing applications (Chen, et al., 2012).

2.2.3 Composites

Composites come into being when more than one material and their properties combine to form one material with synergistic properties. When composites are used as a biomaterial, they are termed as biocomposites. Biocomposites, for the clinical use, are the combination of polymer-polymer, polymer-ceramic or ceramic-ceramic. Scaffold with these combinations have both biological and mechanical properties and is the better substitute over autograft or allograft. (Basha, et al., 2015).

The reason behind designing biocomposites is to overcome the flaws of individual material. Examples of biocomposites with different compositions may include collagen 1 with TCP, self-reinforced polymers (PLLA, PLGA) with calcium phosphate, and collagen 2 with HA bioceramics (Yeo & Kim, 2011). Furthermore, porosity can be induced in composites by different techniques like thermally induced phase separation, wet spinning, and electrospinning to make them applicable in BTE (Al-Qaysi, 2018).

Despite of the many advantages of composites in TE, there remain some challenges that need to be overcome. Firstly, designing of the composites and their variables are very complex as compare to monolithic traditional materials. Satisfactory biocompatibility test of composite implants has not been achieved yet because the response of composites components interacting with each other are not completely understood. Lastly, fatigue behavior of the composite materials after being implanted in the body is difficult to assess than traditional materials like metals and polymers because composite materials are inhomogeneous and anisotropic unlike materials like metals therefore, there can occur different types of damage like fibre fracture, matrix cracking, delaminations etc. independently or interactively. Hence, standards for their examinations are still in progress (Salernitano & Migliaresi, 2003; Degrieck & Paepegem, 2001).

2.3 Bioactive glasses

Professor Larry Hench invented the very first bioactive glass in 1969 at the University of Florida. Its development started with an idea that it would have strong interface with tissues like bone. Professor Hench came up with the glass named 45S5 (Bioglass®) having composition (46.1SiO_2, 24.4Na_2O, 26.9CaO and 2.6P_2O_5) in Mol%. This glass implant appeared to be so strongly bonded with the rat femur bone that bone broke during implant removal. This invention of Professor Hench launched the bioactive glass research field that further allowed the development of new products by varying composition of bioactive glasses that lead to the improvement in processability and bioactivity (Jones,

2013; Hench, et al., 1971; Pacheco, et al., 2015). Bioactive glasses exhibit bioactivity which refers to the ability of the material to bond to host tissue as a result of biological reaction at the interface. After the Hench discovery till now, many of the bioactive glasses with different compositions (mentioned in Table 2) have been developed for various modern and traditional clinical applications. For instance, one of the compositions from the table below, bioactive glass (S53P4) is a special glass developed with the composition ($53SiO_2$, 20CaO, $23Na_2O$, $4P_2O_5$) in wt.% which is utilized in maxillofacial reconstruction such as clinical frontal sinus obliteration, orbital floor reconstruction etc., (Peltola, et al., 2006; Aitasalo, et al., 2001). Similarly, silicate and phosphate based bioactive glasses when doped with metal oxides (Ga_2O_3, Ag_2O and CuO), become useful material for wound healing applications. Therefore, variations in bioactive glasses is needed for different requirements of the clinical applications (Ylänen, 2011).

Table 2. Table shows the different composition of bioactive glass researched globally (Pacheco, et al., 2015).

Composition (wt.%)	45S5	13-93	13-93B3	58S	S53P4	52S4.6	45S5F	S53P4	46S6
Na_2O	24.50	6.00	5.50	0.00	23.00	21.61	24.50	23.00	24.00
K_2O	0.00	12.00	11.10	0.00	0.00	0.00	0.00	0.00	0.00
MgO	0.00	5.00	4.60	0.00	0.00	0.00	0.00	0.00	0.00
CaO	24.50	20.00	18.50	32.60	20.00	21.64	12.25	20.00	24.00
SiO_2	45.00	53.00	0.00	58.20	53.00	50.76	45.00	53.00	46.00
P_2O_5	6.00	4.00	3.70	9.20	4.00	5.99	6.00	4.00	6.00
B_2O_3	0.00	0.00	56.60	0.00	0.00	0.00	0.00	0.00	0.00
CaF_2	0.00	0.00	0.00	0.00	0.00	0.00	12.25	0.00	0.00

Hench's discovered glass was a silicate glass having network of SiO_2 making up the three-dimensional glass structure. 45S5 glass shows bioactivity due to its low content of SiO_2, high glass network modifiers content (Na_2O and CaO) and in addition, high CaO/P_2O_5 ratio (Rahaman, et al., 2011). Glass network modifiers create non-bridging oxygen (NBO) groups which denature the silica glass network. Connection of the silica glass network reduces an increase in the NBO which also results in increased reactivity due to decrement of silicon-oxygen bridges. On the other hand, phosphorus establishes bonds with oxygen atoms like silicone (Ylänen, 2011, pp. 3, 4, 17).

Bioactive glasses have that special features of promoting the bone cells growth and bond to surrounding hard and soft tissues through chemical reactions. These glasses are attractive because by changing their chemical compositions, rate of degradation can be controlled enabling fabrication of glass scaffolds with variable degradation rates with respect to bone ingrowth and remodelling. Moreover, upon their implantation, ions released trigger the osteogenic genes expression and stimulate angiogenesis (Fu, et al., 2011).

When bioactive glass is immersed in biological solution, the chemical reaction takes place at the surface of the glass and, as a result, a HA layer is formed. This HA layer is responsible for the glass bonding to the hard tissue (Rahaman, et al., 2011). The reactive layer adsorbs proteins from the biological fluid on the surface which let the osteoprogenitor cells attach and the process of proliferation and differentiation to the mature osteoblasts takes place (Hench & Polak, 2002). At last, glass degrades, and new bone takes its place. Matching of bone formation with the material degradation is ideally preferred. For better understanding, as an example, whole process of glass-biological fluid interaction including its timeframe is further explained in Figure 3 (Hench, 1998).

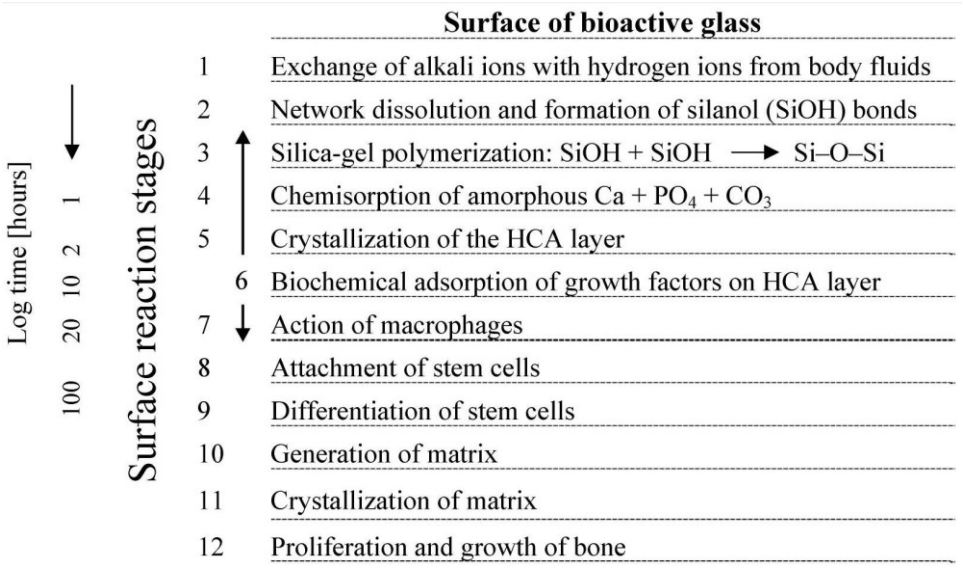

Figure 3. *Reaction steps between bone and implant surface causing the formation of new bone. (Hench, 1998).*

There are two methods by which bioactive glasses are formed i.e., melting process and sol-gel processing. In biomedical applications, usually melt-derived bioactive glasses are utilized (Will, et al., 2012). These glasses come into being after two processes. Firstly, high purity raw materials, mostly carbonates, are homogeneously mixed and melted in a

furnace at temperature between 1000-1500 ºC for time varying between 1-24 hours depending on glass batch size and chemistry (Ylänen, 2011, p. 6). Secondly, molten form of the glass is casted and further annealed. Also, small fragments or frit of the frozen glass can be obtained by pouring the glass-melt into water (Will, et al., 2012, p. 200; Jones, 2013).

The second method for manufacturing glass is the sol-gel processing. In this method, glass is obtained by making a gel using chemistry-based processing such as, condensation and gelation reactions of metal alkoxide in solution. Later the gel turns into glass when heated and drying (Will, et al., 2012). Sol-gel process can be altered by controlling process chemistry and it can be performed at RT. Glass obtained from this process is usually nanoporous with the increased reactivity and decreased mechanical properties (Rahaman, et al., 2011).

2.4 Phosphate Bioactive glasses

Phosphate glasses have been researched over one hundred fifty years (Graham, 1833). History of the simple phosphate glasses and their different structures have been discussed in detail by Brow (Brow, 2000). In biomedical field, these glasses have been researched to be used in the applications like controlled release vehicles of antibacterial ions such as copper, silver, zinc, and gallium and for 3D construction of the muscular tissues (Valappil, et al., 2007). Phosphate based glasses can be shaped into fibres by spinning, for use in soft tissue engineering applications as guides for muscle or nerve repair (Jeans, et al., 2007; Shah, et al., 2005). When Al_2O_3 and Fe_2O_3 are mixed with phosphate glass fibres, they can be employed as cell guides and as reinforcing materials for skeletal muscles regeneration and myotubes formation. Phosphate glass fibres have been tested *in-vivo* as a nerve guide and positive results obtained which termed phosphate glasses as smart materials. (Shah, et al., 2005; Ahmed, et al., 2004c; Kaur, et al., 2013). For BTE, phosphate glasses are regarded as bone tissue regenerative materials in the form of bulk or powders when mixed with polymers in composites materials. (Kaur, et al., 2013).

P_2O_5 as glass forming network and CaO and Na_2O as modifiers, both contributes to form phosphate bioactive glasses. These glasses and bone have the same chemical resemblance as the constituent ions of phosphate bioactive glasses are also present in the organic mineral phase of the bone. Degradation rate of these glasses can be controlled

by simply modifying the glass composition. Thus, phosphate glasses appear to be a potential candidate for biomedical use as resorbable materials (Rahaman, 2014). An apatite-like layer usually termed as calcium phosphate layer forms on the surface of all phosphate bioactive glasses. Its thickness increases with increase in immersion time that allows the adhesion, proliferation and differentiation of cells. According to one study, the presence of SrO and MgO in the apatite layer restrict the leaching of phosphate in the solution which result in increased durability of phosphate glasses (Massera & Hupa, 2014; Massera, 2016). Phosphate bioactive glasses exhibit wide hot working domain which proves their good thermal properties as evidenced by the large amount of phosphate bioactive glass fibres studied in previous years (Ahmed, et al., 2004a; Massera, et al., 2015).

Despite of the vast range of glass compositions, weight loss as a function of time and the concurrent release of ions from the glass remain linear resulting in constant release of ions from the glass during its lifetime. Phosphate bioactive glasses show more controlled rate of dissolution than the silica-based glasses. Silicate bioactive glasses show variation in ions release by the passage of time (Salih, et al., 2000; Ahmed, et al., 2004a).

Structurally, the basic building blocks of phosphates are phosphate tetrahedra which combines to form phosphate networks. Phosphate tetrahedra have different number of bridging oxygens such as cross-linking network (Q^3), polymer-like chain (Q^2+Q^1) or small pyro-(Q^1) and orthophosphate groups (Q^0). Whereas, Q^i terminology is used to classify tetrahedra, in which 'i' represents the number of bridging oxygens (BO) that link tetrahedra with each other as shown in figure 5. (Brow, 2000). P-O bond length varies between BO to non-bridging oxygen (NBO). As phosphate tetrahedra have an average P-O bond length of about 1.54-1.57 Å. Whereas, P-O bond length for BO is about 1.61-1.64 Å, but for NBO, the P-O bond lengths decrease systematically for Q^3, Q^2, Q1 and Q^0 tetrahedra (Ma, 2014).

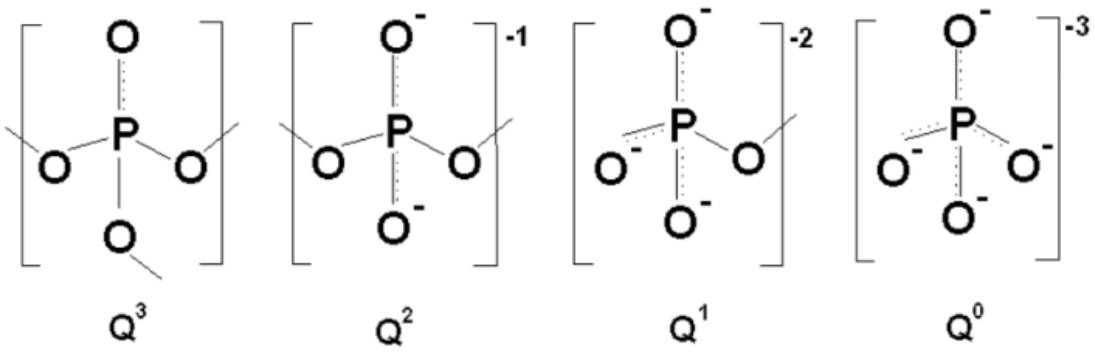

Figure 4. *Example of phosphate tetrahedra in phosphate network (Brow, 2000).*

Phosphate glasses applications and properties are compositions dependant. Though they are commercialized for various applications as they show efficient physical properties including controllable chemical durability in liquid solution, low melting and processing temperatures and high thermal expansion coefficient (Brow & Tallant, 1997; Bunker, et al., 1984). As bioactive (Na_2O-CaO-P_2O_5) glasses have good biocompatibility accompanied by amazing degradable properties with low toxicity and minimal inflammatory response (Ahmed, et al., 2004b; Gough, et al., 2002; Gough, et al., 2003), when copper and silver are added to the phosphate glasses, can be suited for local treatment of the infections (Mulligan, et al., 2003a; Mulligan, et al., 2003b).

2.5 Scaffolds

Scaffolds are defined as porous three-dimensional constructs acting as a substrate in the body to temporarily replace and support parts of tissues by facilitating cells proliferation and differentiation functions that lead to natural healing process of the tissues. There are some necessary requirements for the scaffolds to be fulfilled for use in BTE such as biocompatibility, osteoconductivity, osteoinductivity, osteogenecity, osteointegration, interconnected porosity and mechanical properties. Because success and applicability of BTE are achieved by the performance of the scaffolds (Sultana, 2013; Jones, 2013; Fu, et al., 2011).

Adult mammal is incapable of regenerating tissues fast (except small bone defect) that have been removed or lost as a result of accident or surgery, this is where scaffolds help to accelerate the wound healing process. Scaffolds along with proper cell seeding density and/or growth factors might heal the critical size bone defects. Being an artificial matrix, scaffolds can not only perform as a guide or template for adhesion, growth and function of the cell but also synthesize extracellular matrix (ECM) which results in new tissue generation. Selection of materials to develop the scaffolds as a matrix totally depends upon the final application, whether they will be used as structural support or drug delivery capability or both. Usually polymers, ceramics, and composites are preferred. Ideally, scaffolds should be degraded as new tissue regenerates and replace them naturally (Khan, et al., 2008). Figure 5. presents the key factors involved in scaffolds designing.

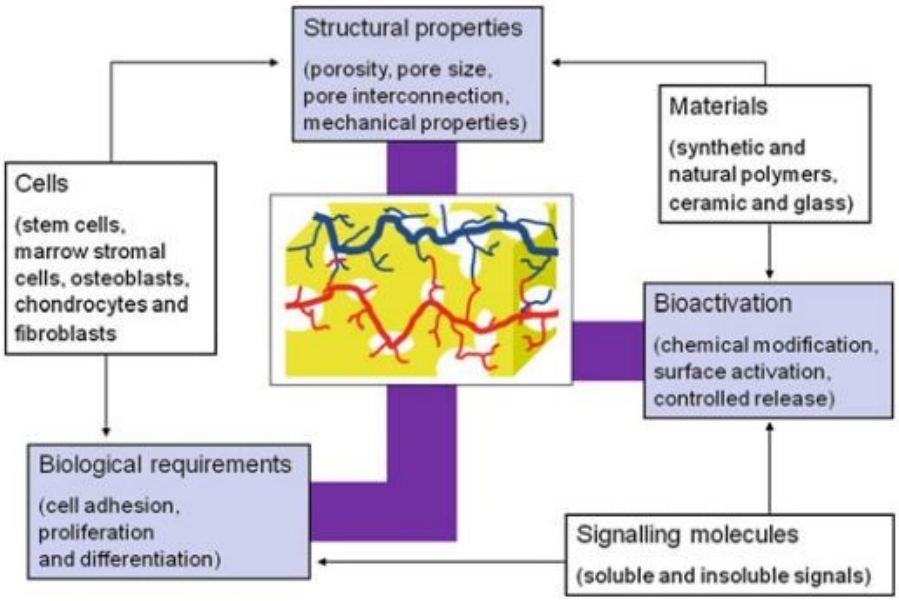

Figure 5. *An illustration of the most important elements to be considered in BTE while designing scaffolds (Will, et al., 2012)*

It is expected from the scaffold material to be biocompatible for cell attachment, proliferation and differentiation. In BTE, more focus is on osteoconductivity and bioactivity while creating the material to facilitates the scaffold-bone bond formation and bone growth, which also prevent the encapsulating fibrous tissue formation (Will, et al., 2012). Regeneration of osseous tissue requires from the scaffold material: a lack of immunogenic response, *osteoconductivity* (the interconnected porous structure allows cells attachment, proliferation and migration through the pores along with the nutrient-waste exchange and penetration of new vessels), *osteoinductivity* (stimulation of new bone growth on the implant away from the bone–implant interface) *osteogenecity* (production of minerals by the osteoblasts at the site of new bone formation to calcify the bone matrix that is responsible for making substrate for new bone), and o*steointegration* (new formed mineralized tissue must bond with implant material) (Khan, et al., 2008; Jones, et al., 2007). Furthermore, an ideal scaffold for BTE has adequate interconnected porosity where cells can migrate, nutrients can be delivered, and cellular waste can be removed. Specifically, size of the pores <50μm is considered essential for cell and protein adhesion, cell migration and osteointegration. Whilst, pores size more than 300μm enables the new bone formation, larger bone ingrowth and vascularization (Will, et al., 2012, p. 200). At least, 50% porosity is required in the scaffold for adequate tissue ingrowth (Rahaman, et al., 2011). It should be noted that where large pores size of the scaffold favors the biological activity, at the same time negatively affects the mechanical properties of the scaffold.

Therefore, compromises are there between mechanical and biological performances (Tomlins, 2016, p. 39; Jones, 2013).

Bones in the different sites of the patient's body possess different physical and mechanical properties, which demands scaffold properties to be altered accordingly for different applications. Furthermore, physical loading affects the bone remodelling therefore, matching of the strength of both scaffold material and bone is necessary to provide sufficient mechanical stimulus but stress-shielding should be avoided at the same time (Sultana, 2013; Fu, et al., 2011).

2.5.1 Scaffold Fabrication Techniques

Since, success of the bone defect treatment is dependent on the properties of the scaffold, therefore, it is necessary to consider the choice of raw materials and optimization of the processing methods. At present, there are no specific fabrication techniques or material that are perfect for all clinical applications (Hutmacher, 2000). Adjustment of the processing parameters for the choice of material is needed to fulfil the scaffolds structure criteria (Tomlins, 2016, pp. 30-34; Hollinger, et al., 2004, pp. 159, 160).Some of the fabrication techniques which are extensively used to produce porous bone scaffolds are chemical/gas foaming, particle/salt leaching, freeze drying, solvent casting, thermally induced phase separation, and foam-gel method. These methods are not efficient when it comes to controlling scaffold shape, pore size and their interconnectivity. Custom designing of the scaffolds for specific application cannot be obtained through these approaches (Bose, et al., 2013). For example, one technique is porogen burn-off method which is one of the oldest techniques used to produce bioactive glass scaffolds. This method employs bioactive glass powder and organic particles, both are mixed and heated which results in decomposition of the organic matter that yield the scaffold with porous structure. Porogen burn-off method is simple and cost-effective in terms of scaffold production but in this process, controlling size distribution of the pores is difficult and also if sacrificial material is not fully evaporated, can negatively affect the sintering process of the scaffolds (Brovarone, et al., 2006; Jones, 2013; Chevalier, et al., 2008).

Currently, most advanced techniques used to produce scaffolds are additive manufacturing (AM) approaches, which were introduced in 1986 by Chuck Hull. These approaches include solid free form fabrication (SFF), stereolithography (SL), rapid prototyping (RP) or robocasting, selective laser sintering (SLS), and fused deposition modelling. In some research papers these techniques are separately described whereas, in others, they are counted as synonyms for single technique. No doubt that they have

gained great scientific interest because scaffolds designed and fabricated via these techniques show controlled shape, pore size, and interconnectivity and also made it possible to easily tailor the scaffold properties by simply changing parameters. In these approaches scaffolds are formed in a layer-by-layer fashion from a computer aided design (CAD) file or text file, without the use of traditional tools such as dies or moulds. (Bose, et al., 2013; Fu, et al., 2011; Baino, et al., 2019). For instance, Tesavibul et al. discovered a special AM method named as lithography-based additive manufacturing technique during his research in producing Bioglass® based scaffolds. This technique proved to be better than SLS and powder-based 3D-printing. In this technique, glass or ceramic parts are produced by processing photopolymer which basically contains a great amount of glass or ceramic particles. Figure 6. Shows scaffold fabricated using lithography-based AM technique (Tesavibul, et al., 2012).

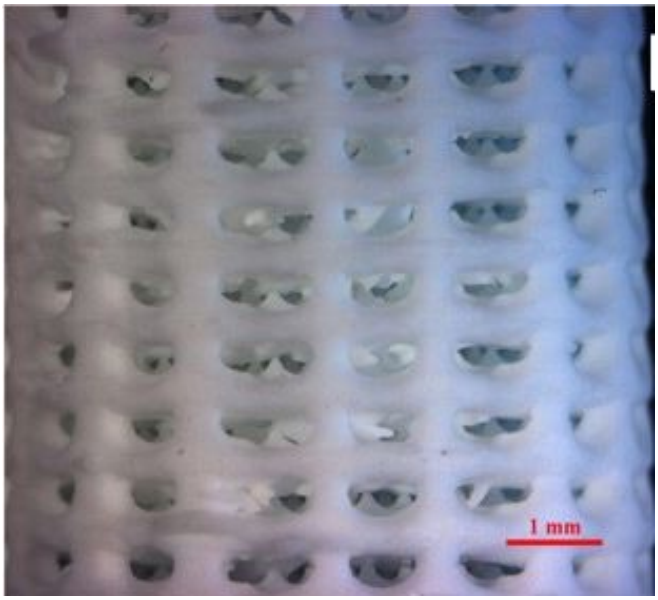

Figure 6. *A picture presents Bioglass® based scaffold produced using lithography-based AM technique. Cropped from (Tesavibul, et al., 2012).*

However, AM techniques have few challenges such as, processing time and require complex and costly equipment. Post-processing is necessary after scaffolds fabrication such as sintering, in which, there is a risk of non-uniform shrinkage of the scaffolds which may cause cracking in the scaffolds parts. Also, selection of the binders in the material and their removal during the sintering are great challenges to be considered. Despite of these limitations, AM techniques have great potential in the future requiring extensive optimization before the high-quality parts can be made (Bose, et al., 2013; Ylänen, 2011, p. 168; Woodruff & Hutmacher, 2010).

2.5.2 Robocasting of Bioactive glass scaffold

Currently, information found in the literature about the production of bioactive glass scaffolds is limited using additive manufacturing approaches. Robocasting technique, however, seems to be powerful and commonly adopted technique for fabrication of glass and glass-ceramic scaffolds. In this direct-writing method, robot-controlled nozzle extrudes ink continuously in the form of filament in a 3D fashion (layer-by-layer) on the surface of building platform to construct three-dimensional structure. Printing ink, which is a slurry, made up of either glass or ceramic powders with the polymeric binder usually Pluronic F-127. It is characterized by appropriate rheological properties. Rheological properties of the ink are defined by its viscosity, yield stress and dynamic elastic modulus. In robocasting, Pluronic F-127 has been preferred widely as a binder in BTE applications (Baino, et al., 2019; Eqtesadi, et al., 2014).

Recently, scaffolds based on silicate bioactive glass (47.5B glass) were fabricated using robocasting technique for bone regeneration application. Scaffolds had grid-like structure and were highly bioactive and amorphous (Baino, et al., 2019). Before that in 2017, Mattioli-Belmonte et al. obtained porous multilayer glass-PLGA composite 2D and 3D bone like scaffolds using robocasting technique named as pressure-activated microsyringe (PAM) method. Scaffolds were resembling to the topological features of the cancellous bone. 3D Scaffolds were successful in aiding proliferation of osteoblast-like cells and periosteal-derived scaffolds, showing their applications in bone tissue engineering (Mattioli-Belmonte, et al., 2017).

In the history, Franco et al. were the first who obtained bioceramic scaffolds using robocasting technique in 2010, their ink was based on ceramic to build HA, β-tricalcium phosphate (β-TCP), and biphasic (HA/β-TCP) structures (Franco, et al., 2010). Later, robocasting came in trending where commercial glass i.e., 45S5 Bioglass® and 13-93 glass were processed using this technique by many other researchers. Silicate 13-93 bioactive glass was produced by Liu et al. in 2013 utilizing robocasting technology to evaluate the mechanical properties of the obtained scaffolds. Scaffolds were grid-like microstructured, having 300μm pore width and 47% porosity. Compression tests and flexural loading were carried out before and after their immersion in SBF *in-vitro* and in rat subcutaneous model in vivo. Scaffolds compressive strength was reduced after 2 weeks of immersion in SBF and in vivo implantation. Furthermore, brittle mechanical response shifted to elastoplastic response was observed longer than 2-4 weeks in vivo. These strong porous scaffolds Showed promising result for loadbearing application or loaded bone repair (Liu, et al., 2013).

In 2014, Eqtesadi et al. obtained 45S5 Bioglass® robocast scaffolds having interconnected porosity under 60 to 80% for a fixed scaffold design. Compressive strength of those scaffolds were similar to that of cancellous bone (2-13MPa), even after sintering below the crystallization temperature. He admitted that robocasting technique is the only technique which can provide with the scaffold, customized external geometry and optimized pore architecture (Eqtesadi, et al., 2014). One more 45S5 Bioglass® scaffold was fabricated in 2017 via robocasting technique to investigate the effect of different postprocessing thermal treatments on the scaffold mechanical response by sintering both amorphous and crystallized scaffolds. Cell culture tests revealed that crystallization caused by sintering scaffolds at 1000ºC enhanced cells proliferation and long-term viability in vitro (Motealleh, et al., 2017).

3. MATERIALS AND METHODS

In this chapter, experimental part of the thesis is explained where first, phosphate bioactive glasses were produced to analyse their properties and select the best glass composition(s). Then scaffolds fabrication and their characterization are discussed in detail.

3.1 Glass production and characterization

3.1.1 Glass preparation

Phosphate glass batches with the composition; $45P_2O_5$, $2.5B_2O_3$, $2.5SiO_2$, $10Na_2O$, 20CaO, (20-x)SrO, xMgO in Mol% (x = 0, 5 ,10, 15 and 20), presented in Table 3, for each batch were prepared by homogeneously mixing high-purity raw chemicals; $NaPO_3$, $Ca(PO_3)$, NH_6PO_4, $SrCO_3$, MgO, H_3BO_3, and SiO_2 in a mortar and transferred to the platinum crucible. Chemicals mass were calculated to get 15 grams of glass.

Table 3. *Compositions of the glasses in (Mol%)*

Glass	P_2O_5	B_2O_3	SiO_2	Na_2O	CaO	SrO	MgO
X = 0	45	2.5	2.5	10	20	20	0
X = 5	45	2.5	2.5	10	20	15	5
X = 10	45	2.5	2.5	2.5	20	10	10
X = 15	45	2.5	2.5	2.5	20	5	15
X = 20	45	2.5	2.5	2.5	20	0	20

Every mixture transferred in a platinum crucible was melted in air in an LHT 02/17 LB speed electric furnace (Nabertherm GmbH, Lilienthal, Germany). The melting temperature was set to 1200°C and the ramp was set to 10°C/min. Final temperature was maintained for 30 minutes.

The melt was then casted in a brass mould and allowed to solidify a little bit after which the semi-solid glass was placed in a pre-heated electric muffle furnace (Nabertherm L 5/11 or L 3/12) for annealing at 400°C for 5 hours to reduce the internal stress. Post-annealing solid glass was brought to the RT inside the furnace overnight. The glass melting thermal profile can be seen in Figure 7.

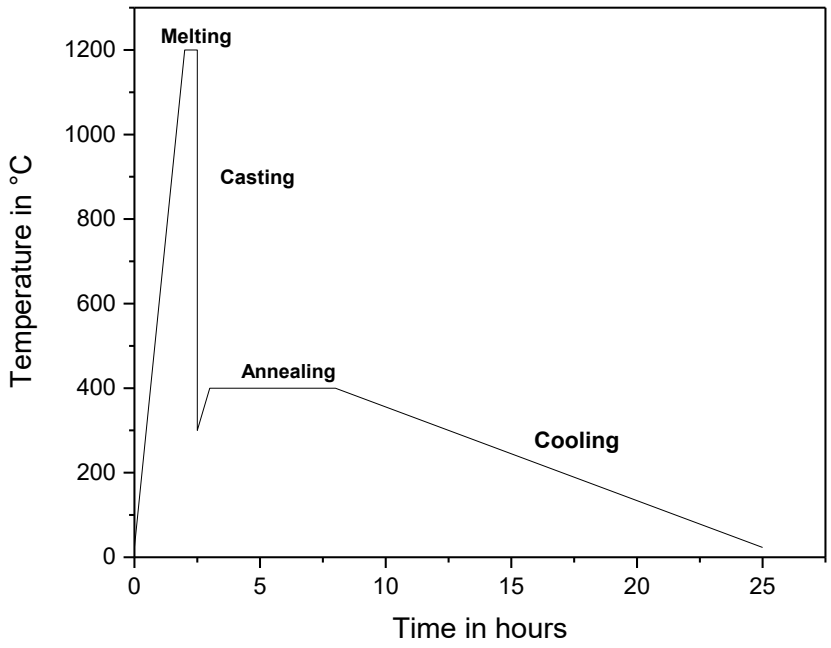

Figure 7. *Pictorial representation of thermal processes for glass formation.*

Next day, glass was taken out of the annealing furnace and crushed in metallic mortar and sieved in ASTM specified test sieves (Gilson Company, Inc., Ohio, USA) to get at least 3.5 grams of 125-250μm and <38μm particle size powders. Desired amount was obtained and stored in a tube, in a desiccator for the characterization.

3.1.2 Thermal properties

In order to determine the thermal properties of the glasses, thermal transitions of the glasses were investigated by performing Differential Thermal Analysis (DTA) on 125-250μm and <38μm sized glass particles using STA 449 F1 Jupiter® (Netzsch-Gerätebau GmbH, Selb, Germany) machine. A platinum crucible was filled with 28mg of glass powder and heated at a rate of 10 °C/min from 40-800°C under 50 ml/min flow of Nitrogen. The T_g (glass-transition temperature), T_x (onset of crystallization temperature) and T_p (crystallization temperature) were revealed by the obtained DTA curves in origin software. T_g was considered as the inflection point of the first endothermic event taken from the minimum of the first derivative of the DTA curve. T_x was taken as the onset of the crystallization peak, using the tangent method. T_p was taken as the maxima of the crystallization peak. The accuracy was about ±3°C. The hot working window ΔT was calculated using the formula ($\Delta T = T_x - T_g$).

3.1.3 *In-vitro* dissolution test of glasses

In-vitro dissolution test of both powder sizes (125-250µm and <38µm) was conducted in Simulated Body Fluid (SBF) to examine the bioactivity of the glass for 24h, 48h, 72h, 1 week and 2 weeks.

Before the test, SBF solution was prepared according to the recipe proposed by Kokubo (Kokubo & Takadama, 2006). SBF was obtained after slowly mixing the analytical grade chemicals such as NaCl, $NaHCO_3$, KCl, $K_2HPO_4 \cdot 3(H_2O)$, $MgCl_2 \cdot 6(H_2O)$, 1M HCl, $CaCl_2 \cdot 2(H_2O)$, Na_2SO_4 and $(CH_2OH)3CNH_2$ (Trizma® base) in distilled water. Chemicals and their amount used in making SBF are mentioned in the Table 4. After chemicals were properly mixed in the distilled water, the volume of SBF was adjusted to 1L and pH was set to 7.40 ±0.02 at 37ºC. Ionic concentration of the SBF can be seen in Table 5. SBF solution was stored in a fridge.

Table 4. Chemicals and their quantities for making SBF

Chemicals	Quantity
NaCl	7.996 g
$NaHCO_3$	0.350 g
KCl	0.224 g
$K_2HPO_4 \cdot 3(H_2O)$	0.228 g
$MgCl_2 \cdot 6(H_2O)$	0.305 g
1M HCl	40 ml
$CaCl_2 \cdot 2(H_2O)$	0.368 g
Na_2SO_4	0.071 g
$(CH_2OH)_3CNH_2$	6.057 g

Table 5. Ions and their concentrations in the Simulated Body Fluid. Modified table from (Kokubo & Takadama, 2006)

Ions	Concentration in SBF (mM)
Na^+	142.0
K^+	5.0
Mg^{2+}	1.5
Ca^{2+}	2.5
Cl^-	148.8
HCO_3^-	4.2
HPO_4^{2-}	1.0
SO_4^{2-}	0.5

Dissolution test of the phosphate bioactive glasses was carried out by immersing 75mg of powders of each particle size (125-250µm and <38µm) and composition in 50ml of SBF in the 120ml of polypropylene (PP) containers (Sarstedt AG & Co, Nümbrecht, Germany) as per the protocol proposed by Maçon *et al.* (2015). The *in-vitro* dissolution test was done in triplicate. The specimens were left in an orbital Multitron AJ 118 g (Infors, Bottmingen, Switzerland) shaker incubator at 37°C at 100 rpm for up to 2 weeks. After each time point, samples were taken out of the shaker and their pH were measured using S47-K SevenMultiTM pH-meter (Mettler-Toledo LLC, Ohio, USA) at temperature 37.0 ± 0.2 °C. 1 ml of the solution was extracted from each sample and mixed with 9 ml of Ultrapure 1M HNO_3. Glass powders were filtered from the solutions using filter paper with the pore size less than 8 µm then gently washed with acetone and left to dry overnight at room temperature for FTIR-ATR analysis. Ionic concentrations of B, Ca, Mg, P, Si and Sr in the SBF solutions were obtained by analyzing the solution using inductively-coupled plasma—optical emission spectrometer (Agilent Technologies 5110 inductively coupled plasma-optical emission spectrometer (ICP-OES), Santa Clara, CA). Na concentration was avoided due to the high initial amount in the SBF solution. For ion concentration various wavelengths were used, summed up in Table 6, due to potential interaction between some of the lines used. Results were expressed by taking average ± standard deviation (SD) from the triplicate samples at each time point.

Table 6. Ions and corresponding wavelengths used in ICP evaluation.

Ions	B	Ca	Mg	P	Si	Sr
Wavelengths (nm)	249.678	393.366	279.553	213.618	250.690	216.596

3.1.4 Structural properties

All the glass powders (125-250 µm and <38 µm particle size) before and after immersion into SBF underwent Fourier transformation infrared spectroscopy (FTIR) to study the structural properties of glasses. The IR spectra of the glass particles were obtained using Perkin Elmer Spectrum One FTIR Spectrophotometer in Attenuated Total Reflectance (ATR) mode. Every spectrum was the average of 8 scans with the resolution of 1 cm^{-1} in the wavenumber range 600-4000 cm^{-1}. All spectra were normalized to the maximum intensity band and baseline corrected.

3.1.5 Sintering of glass powder

Based on characterization of all glass compositions, two glass compositions were selected to be used in producing scaffolds, i.e. x=10 and x=15. Sintering was conducted on <38µm particle size powder of both compositions to reveal optimum sintering temperature before crystallization occurs. Pellets were obtained by filling a metallic mould with glass powder and applying 25 MPa of pressure using a hydraulic press. The pellets were heat treated in a Nabertherm LT 9/11/SKM electric muffle furnace. Heating was done in an air atmosphere with a heating rate of 3°C/min. Temperatures were raised from RT to 480, 490, 495, and 500 °C and kept at the sintering temperature for 1 hour before being allowed to cool down overnight. Resulting samples were subjected to a wide-angle X-Ray diffraction (XRD; 2θ within 10–70°) analysis using MiniFlex™ (Rikagu, Tokyo, Japan) after being crushed into fine powders to see if crystallization occurred during the heat-treatment.

3.2 Scaffold fabrication and characterization

3.2.1 Glass preparation for scaffolds

In order to get the glass powders for scaffolds, 120g of glass was prepared and crushed using a ball mill, Pulverisette type 05. 102 planetary ball mill (Fritsch GmbH, Idar-Oberstein). For crushing, the ball mill cycle was set to two cycle of 2 minutes at 800 rpm, with a pause of 5 minutes in between cycles. The powder was then sieved to obtain particles less than 38µm.

3.2.2 Physical properties

Density measurement of the glass is crucial in ink preparation for robocasting scaffolds. Therefore, small piece of bulk glass from each composition was taken and density was measured using Archimedes' principle. Firstly, mass of the glass piece was measured in air then glass piece was immersed in the liquid (ethanol 96%vol) free of bubbles and the mass was measured. The glass density ρ_{glass} (g/cm^3) was calculated using the equation mentioned below.

$$\rho_{glass} = \frac{m_{air}}{m_{air} - m_{liquid}} \times \rho liquid \quad (1)$$

Where m_{air} and m_{liquid} are the masses of the glass piece measured in the air and in liquid, and ρ_{liquid} is the density of ethanol 96%vol used as immersion liquid at RT. Five parallel measurements of each glass were obtained and average ± SD are reported.

3.2.3 Scaffold robocasting

Prior to the fabrication of scaffolds, ink was prepared through two steps. In first step Pluronic solution which works as a binder was made by dissolving Pluronic® F-127 (Sigma-Aldrich, CAS No. 9003-11-6) in a plastic container filled with distilled water to obtain a concentration of 25% by weight. Plastic container was covered with ice in an ice-bath and that bath was placed to a magnetic stirrer at room temperature keeping the stirring rate at 100-150 rpm. Ice in the bath was refilled when needed to keep the temperature low around the solution and to facilitate the homogeneous dissolution of Pluronic. When the Pluronic solution was clear and transparent, it was stored in the fridge below 4°C temperature in a sealed container. Mass of the Pluronic F-127 in the solution was determined according to the equation 2 below.

$$Mass\ of\ Pluronic = Pluronic\ density \times percentage\ of\ Pluronic \times Multiplying\ factor \quad (2)$$

In the second step, ink with 35 vol.% glass concentration was prepared by adding Pluronic solution drop by drop to the glass powder in the plastic pot followed by alternating vigorous vibrating mixing around 2500 rpm using Vibrofix VFI electrical shaker (IKA® - Laboretechnic, Saufen, Germany) for 6-7 times with 1 minute mixing and 30 seconds cooling in the ice-bath between each mixing turn. After the mixing was done and homogeneous mixture was obtained, visible bubbles were reduced by tapping the ink to get bubble free slurry. Ink was transferred in the syringe and exceeding air was removed by pushing the piston against the opening of the syringe. Plunger was inserted in the cartridge and pressed it to the bottom then adaptor was used to connect both syringe and cartridge followed by transferring ink from syringe to the cartridge while acted on plunger to avoid transferring air in the cartridge. Tip of the cartridge was sealed with parafilm and let it be stabilized for 1 hour in room temperature before printing. Again, here mass of the glass in the ink was determined using the equation 3.

$$Mass\ of\ glass = glass\ density\ \times percentage\ of\ glass \times multiplying\ factor \quad (3)$$

The multiplying factor is defined as a fixed integer number that has to be adjusted depending on the density of the material used in order to completely fill the cartridge for printing. The lower is the density of the material, higher is the multiplying factor.

After 1 hour of ink stabilization, robocasting was performed using 3Dn-Tabletop (nScrypt Inc., Orlando, Florida, USA) which was controlled by the Machine Tool 3.0 system software. Plastic tips (Nordson EFD Optimum® SmoothFlow™ tapered dispensing tips) with a diameter of 410µm which are designed for the ink extrusion were attached with the cartridge front opening and cartridge was fixed to the printing head with the labelled tube attached at the back for pressure exertion. Printing height of the scaffold was determined by the printing head which was allowed to move only in z-axis whereas, printing table under the head was moving in x and y-axis with respect to the printing head to achieve the extrusion. Acetate sheets (Colour Copier and Laser Transparency OHP Film, Folex AG, Seewen, Switzerland) were placed on the printing table as a substrate for scaffold printing due to their flatness, good adhesions with the ink and easiness in detachment of the scaffolds from them once they are dry (Baino, et al., 2019).

Processing parameters were entered in the software to get the scaffolds of desired properties where the movements of the printing table in x- and y-direction were according to the script, written in text file. Speed of displacement was set to 4 mm/s. Pressure for the material feed was in the range of 15-18 psi, to maintain constant ink flow from the cartridge to the sheet. Scaffold with size of 3.7×3.5 mm (20 layers), every next layer deposited onto the previous layer was rotated to 90º angle to get porous and cylindrical grid

like structure. After scaffolds were printed, they were left to dry in RT for 24 hours and then removed from the acetate sheet.

Optimized sintering temperature from previous test was used to sinter the 3D printed scaffolds.

3.2.4 *In vitro* dissolution test of scaffolds

The bioactivity of the scaffolds was analysed by using the same protocol mentioned in subchapter 3.1.3, but this time there were scaffolds instead of glass powders. Three parallel samples of both glass scaffolds compositions along with three blank SBF samples as a control were incubated for 6h, 24h, 48h, 72h, 1week and 2weeks in 120 ml of SBF. The mass of the samples was measured before and post immersion, as dry and the mass was quantify using the equation 4.

$$Mass\ loss = \frac{\Delta W}{W_0} = \frac{W_0 - Wt}{W_0} \cdot 100 \quad (4)$$

W_0 represent the initial weight and W_t is the post-immersion weight of the scaffolds.

At each time point the pH of the solutions was measured and 1 ml of SBF was diluted into 9 ml of 1M HNO_3 for ion concentration measurements.

3.2.5 Physical and structural properties

Scaffold parallel samples before and after immersion time were ground to fine powder and their structural information were examined by FTIR analysis using the same protocol as for powders before robocasting explained in previous subchapter. X-Ray diffraction was performed on both compositional sintered scaffolds to confirm that the selected sintering temperature was any good to avoid crystallization after robocasting scaffolds.

3.2.6 Mechanical Test

Three parallel scaffold samples before and after immersion time underwent mechanical testing using Instron ElectroPuls™ E1000 (All-Electric Dynamic Test Instrument, USA) machine interfaced with the Instron Console software to examine the compressive strength. Cross-head speed was kept as 5 mm/min and the cell load as 5 kN. Before crushing, scaffolds dimensions were measured with the caliper, diameter and height were in the range of 4-5 mm. Compressive strengths of the scaffolds were described by taking the maximum compression values from each measurement. Results were expressed as average ± SD.

4. RESULTS AND DISSCUSION

In this chapter, results obtained from the experiments done in the thesis project are presented and discussed. Phosphate glasses with compositions; $45P_2O_5$, $2.5B_2O_3$, $2.5SiO_2$, $10Na_2O$, 20CaO, (20-x)SrO, xMgO in Mol% (x = 0, 5 ,10, 15 and 20) were prepared. They were studied in light of their thermal, structural and *in-vitro* properties. The most promising glasses were 3D printed into scaffolds and their *in-vitro* dissolution in static condition were assessed.

4.1 Analysis of glass

4.1.1 Thermal properties

Thermal properties of the glasses with both particle sizes i.e., <38µm and 125-250µm are illustrated in DTA thermograms (Figure 8 (a) and (b)). With an increase in MgO content in the glass compositions, T_g and T_p are increasing linearly, whereas T_x remains almost constant within the accuracy of ±3°C in these glass compositions and both particle sizes. Hot working window (ΔT) of the glass x = 0, 5 and 10 also remained almost same. Above 10 mol% of MgO content in the glass shows no crystallization peak which can be evidenced in x = 15 and 20. All values are presented in Table 7 and 8.

Thermal properties of phosphate bioactive glasses rely strongly on their structural features such as crosslinking density, phosphate chain, bonding strength (Shih & Chin, 2001) and composition (Neel, et al., 2009). Thus, shifting of T_g and T_p towards higher temperature with increasing of MgO content (Table 7 and 8) is attributed to the replacement of Sr-O bond with Mg-O bond. Increasing of T_g and T_p is due to the higher ion potential of the Mg^{2+} ions and can be explained by the Dietzel's ionic field strength as ($I = \frac{Z}{r^2}$) where Z represents cation charge and r is the radius. Mg^{2+} has 4.73 $Å^{-2}$ ionic field strength which is higher than other cations present in the glasses especially the cation (Sr = 1.56 $Å^{-2}$) it is replacing (Ma, et al., 2012; Mishra, 2019). This leads to a higher tendency of attracting NBO and increase the rigidity of the phosphate network. This behaviour is in the agreement with the study done by Islam *et al.* where magnesium was replaced with calcium in phosphate glass and resulted in a decrease in T_g and T_p. (Islam, et al., 2017).

(a)

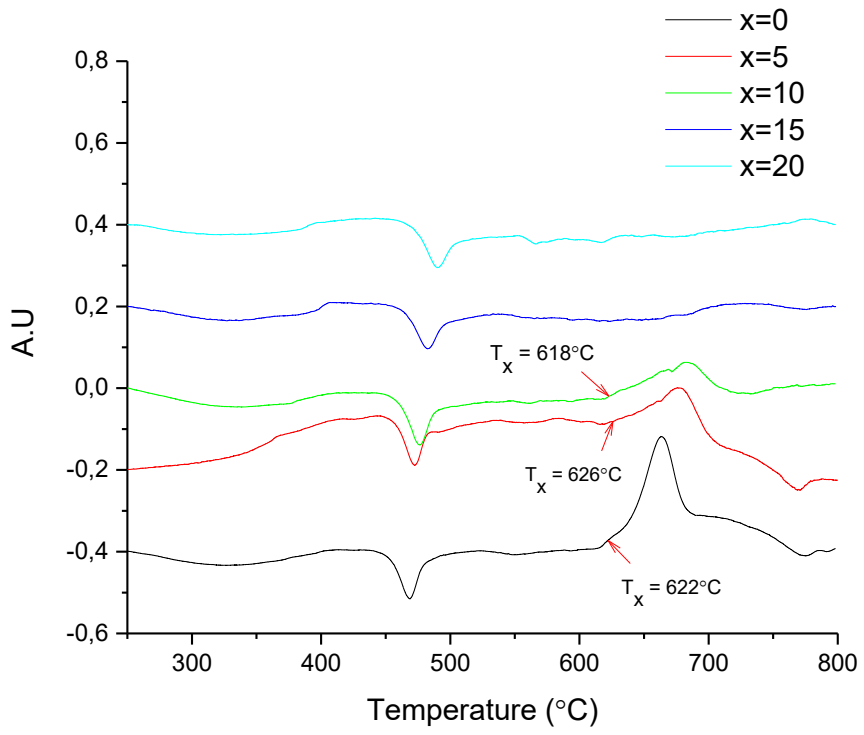

(b)

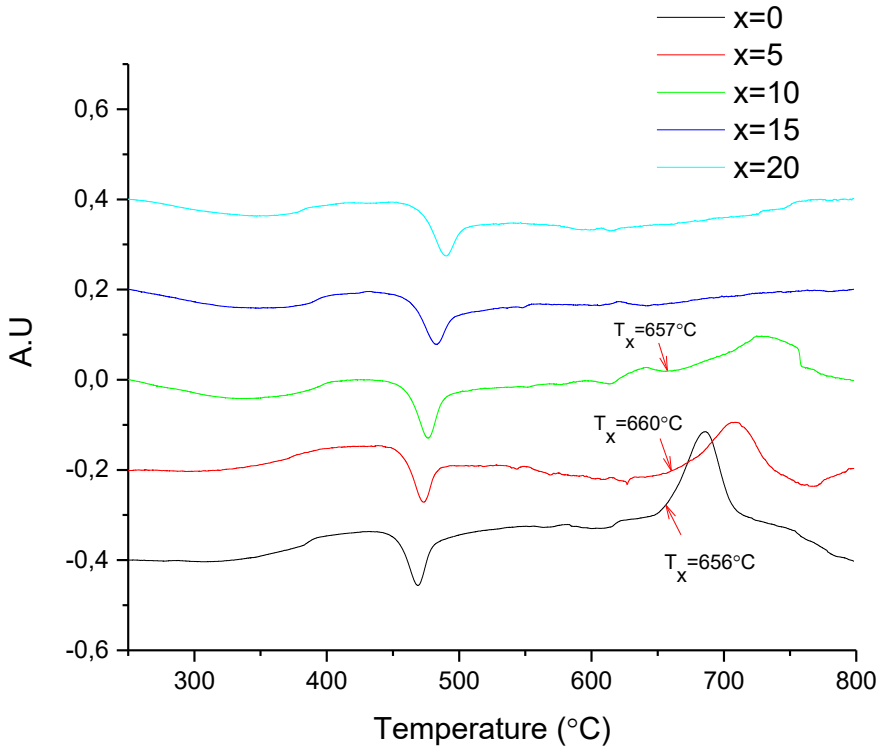

Figure 8. *DTA thermograms of glass (a) <38μm particle size and (b) 125-250μm particle size.*

Table 7. T_g, T_x, T_p and ΔT of glasses having <38μm particle size.

Glass	T_g (°C) ±3°C	T_x (°C) ±3°C	T_p (°C) ±3°C	$\Delta T = T_x - T_g$ (°C) ±6°C
x = 0	463	622	663	159
x = 5	466	626	676	160
x = 10	469	623	682	154
x = 15	475			
x = 20	483			

Table 8. T_g, T_x, T_p and ΔT of the glasses having 125-250μm particle size.

Glass	T_g (°C) ±3°C	T_x (°C) ±3°C	T_p (°C) ±3°C	$\Delta T = T_x - T_g$ (°C) ±6°C
x = 0	463	656	685	193
x = 5	467	660	708	193
x = 10	469	657	728	188
x = 15	475			
x = 20	482			

Form the Figure 8 (a and b) and Table 7 and 8, one can notice that the T_x of all glass compositions having particle size 125-250µm is higher than the T_x in particle size <38µm. This behavior is in the agreement with the Chatzistavou *et al.* study in which they studied 5 different particle sizes of the bioactive glass and studied thermal behavior of all the particle sizes. The thermal analysis revealed that the larger particle sizes were able to drag the crystallization temperature to the higher temperature which was assumed to be due to particle size effects in heat transfer (Chatzistavrou, et al., 2006). However, it should be noted that the dependence of T_p on particle size cannot readily give the information regarding the nature of crystallization mechanism i.e., whether it is surface crystallization or internal crystallization (Ray, et al., 1996). The change in peak temperature as a function of glass particle size indicates the surface crystallization. Surface crystallization mechanism is dominant on small particle size. Therefore, based on previous studies it is expected that the crystallization in small particles are from the surface (Massera, et al., 2012). In the case of x = 15 and x = 20, where no crystallization peaks appeared is because the kinetics of nucleation and growth are so slow that they are not observed in DTA within the time of measurement. ΔT provides the gauge of the resistance to the crystallization, therefore, glass with ΔT higher than 100°C have enough stability to be sintered without any significant crystallization (Massera, et al., 2015). Evidently, In all glass compositions, ΔT is larger than 150°C.

4.1.2 Structural properties

Structural properties of all glass compositions having particle size <38µm were analyzed using FTIR spectroscopy. Obtained spectra were normalized to the band with higher intensity which is located at ~887 cm^{-1}. In Figure 9, there are all together 5 bands present in the spectra at wavenumbers around 1240, 1080, 887, 775 and 718 cm^{-1}, and a shoulder at ~980 cm^{-1}. Absorption bands can be assigned to the phosphate glass network. The bands at around 718 and 775 cm^{-1} can be attributed to P-O-P symmetric stretching in metaphosphate structure (LEE, et al., 2009). The highest absorption band located at ~887 cm^{-1} can be attributed to the P-O-P asymmetric stretching vibration of bridging oxygen in metaphosphate structure (v_{as} P-O-P Q^2) (Shih & Shiu, 2007; Moustafa & El-Egili, 1998). The shoulder located at ~980 cm^{-1} and band at ~1080 are assigned to the symmetric and asymmetric stretching vibration of PO_3^{2-} in Q^1 units. The band peaking at around 1240 cm^{-1} corresponds to the asymmetric vibration of PO_2^- in Q^2 units (Gao, et al., 2004; Neel, et al., 2009).

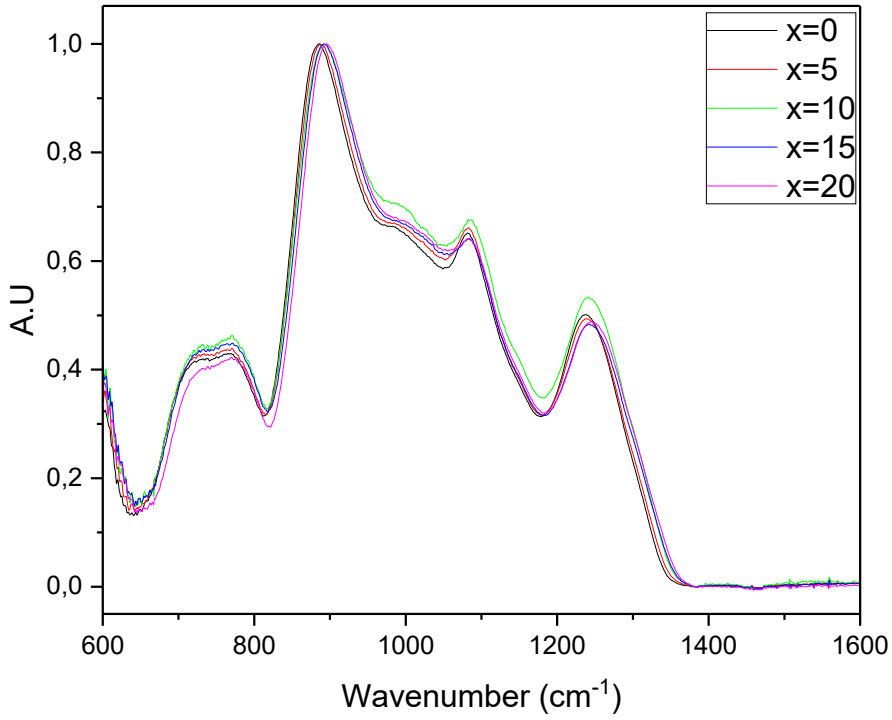

Figure 9. *FTIR spectra of all glass compositions with <38µm particle size*

In a pure phosphate network, PO_3^{2-} tetrahedral units are connected with each other by three bridging oxygens. The network is disrupted when a modifier oxide is added and modifier oxide's cations take the interstitial positions in the network (Carta, et al., 2007). It is observable that the increasing of MgO content didn't change the bands in all compositions in terms of shape and intensity, x = 10 is an experimental error. However, the position of the bands is shifting progressively from lower wavenumber to higher wavenumber that might indicate a strengthening of the bonds due to the smaller ionic radius of Mg^{2+} i.e., 0.72 Å compared to the cations it replaces i.e., Sr^{2+} (1.26 Å) (Shannon, 1976). All bands attribution is summarized in Table 9.

Table 9. Summary of FTIR-ATR bands attributions

Wavenumber (cm^{-1})	Attribution	Reference
718-775	v_s P-O-P in Q^2	(LEE, et al., 2009)
887	v_{as} P-O-P in Q^2	(Shih & Shiu, 2007; Moustafa & El-Egili, 1998)
980	v_s PO_3^{2-} in Q^1	(Gao, et al., 2004; Neel, et al., 2009)
1080	v_{as} PO_3^{2-} in Q^1	(Gao, et al., 2004; Neel, et al., 2009)
1240	v_{as} PO_2^{-} in Q^2	(Gao, et al., 2004; Neel, et al., 2009)

4.1.3 *In-vitro* dissolution test

Dissolution studies were conducted for all glass compositions and for both particle sizes by immersing in SBF for 0, 1, 2, 3, 7 and 14 days to evaluate the impact of increasing MgO content on the ion release mechanism of the glass.

Figure 10 (a) and (b) show the changes in pH of the solutions as compared to the pH of blanks SBF as a function of immersion time. Solution's pH was similar for all glass compositions. However, while the pH does not exhibit any significant change within the accuracy of the measurement for the larger particle sizes, particles <38µm (Figure 10a) exhibit a drop in pH at day 2, and then remained constant within the accuracy of the measurement. So, these glasses upon dissolution remained at the physiological pH.

(a)

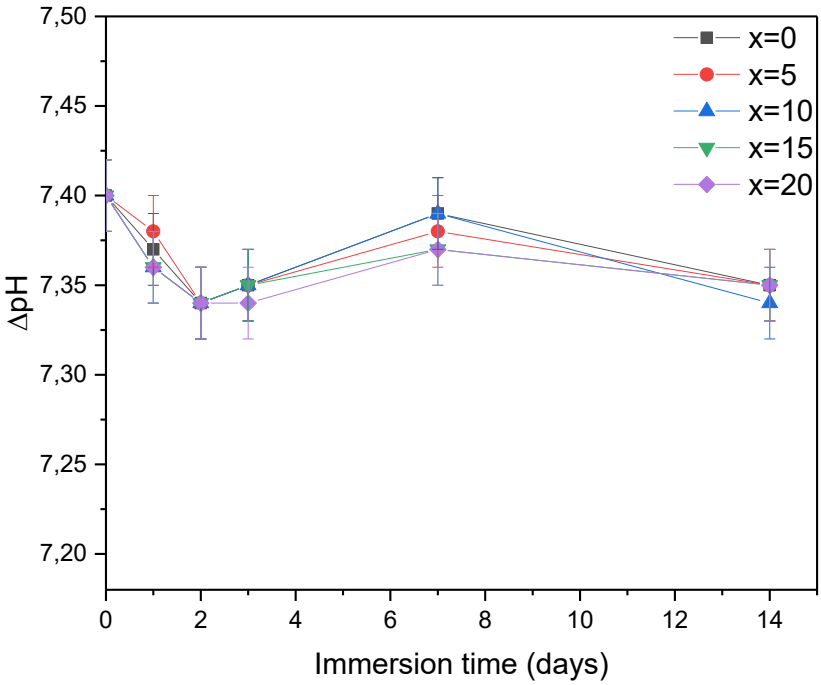

(b)

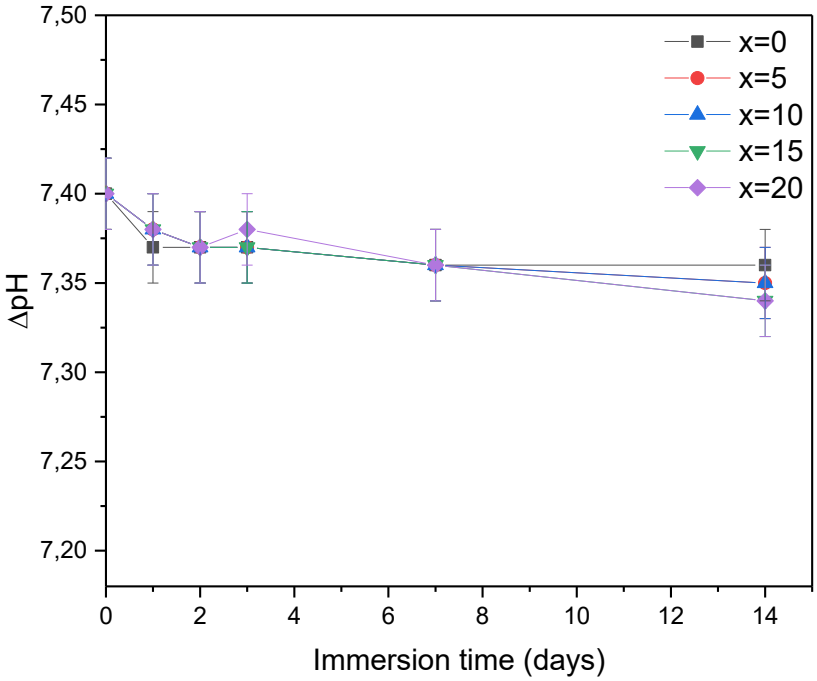

Figure 10. *Change in pH as a function of immersion time of the particle sizes (a) <38μm (b) 125-250μm*

(a)

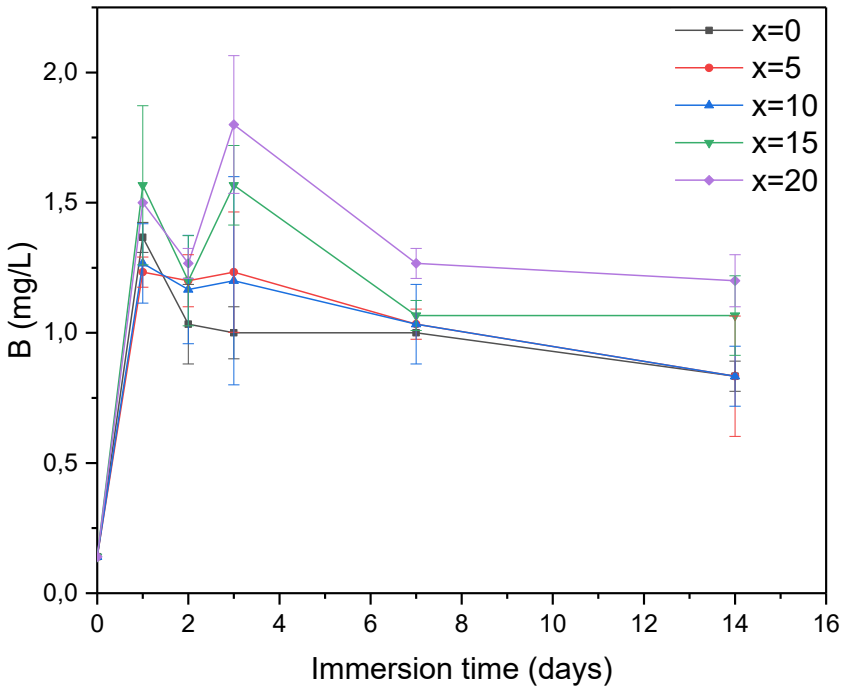
x=0
x=5
x=10
x=15
x=20
B (mg/L)
2,0
1,5
1,0
0,5
0,0
0
2
4
6
8
10
12
14
16
Immersion time (days)

(b)

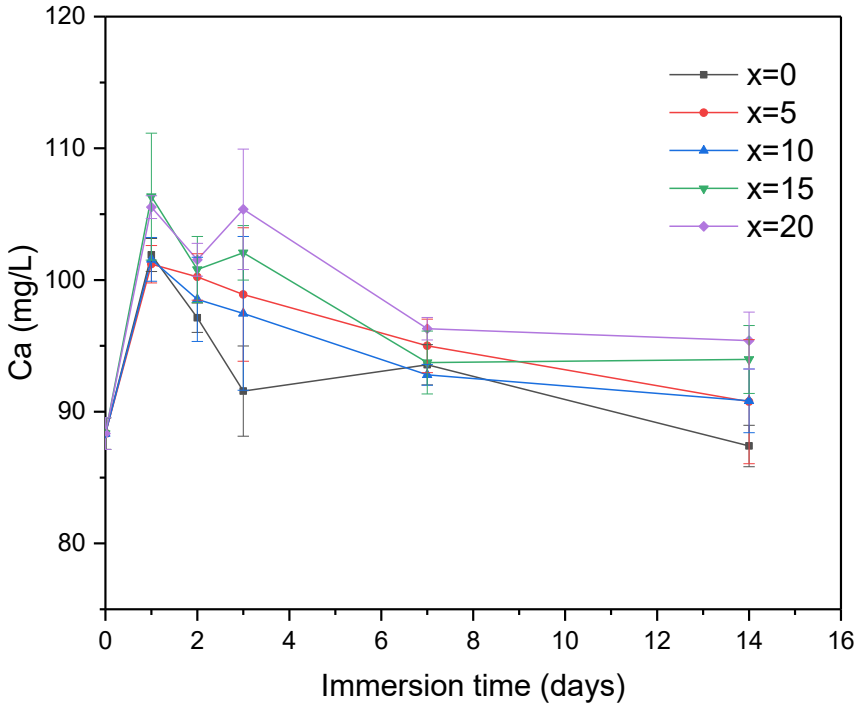
x=0
x=5
x=10
x=15
x=20
Ca (mg/L)
120
110
100
90
80
0
2
4
6
8
10
12
14
16
Immersion time (days)

(c)

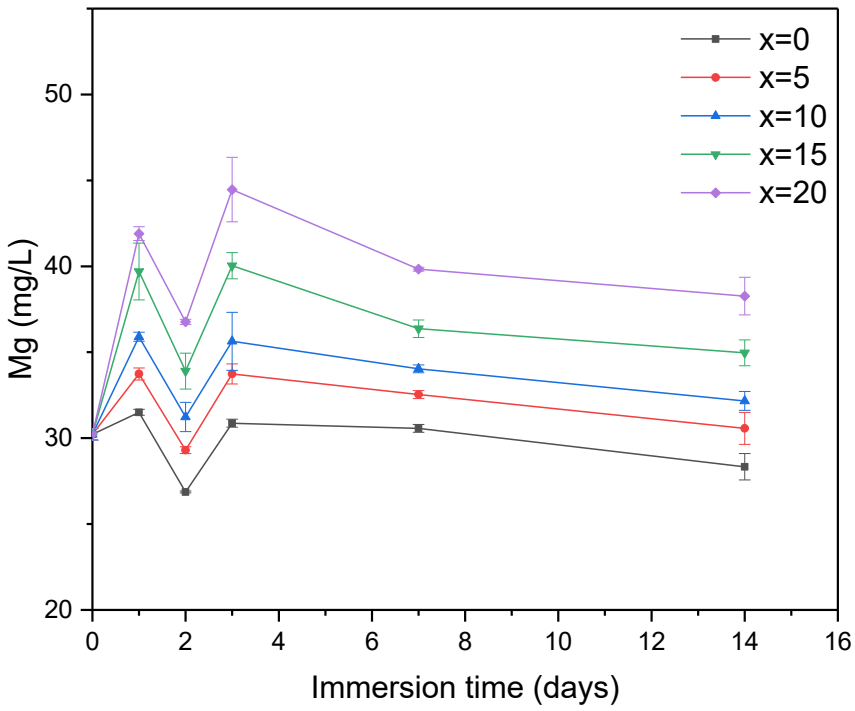
x=0
x=5
x=10
x=15
x=20
Mg (mg/L)
Immersion time (days)
20
30
40
50
0
2
4
6
8
10
12
14
16

(d)

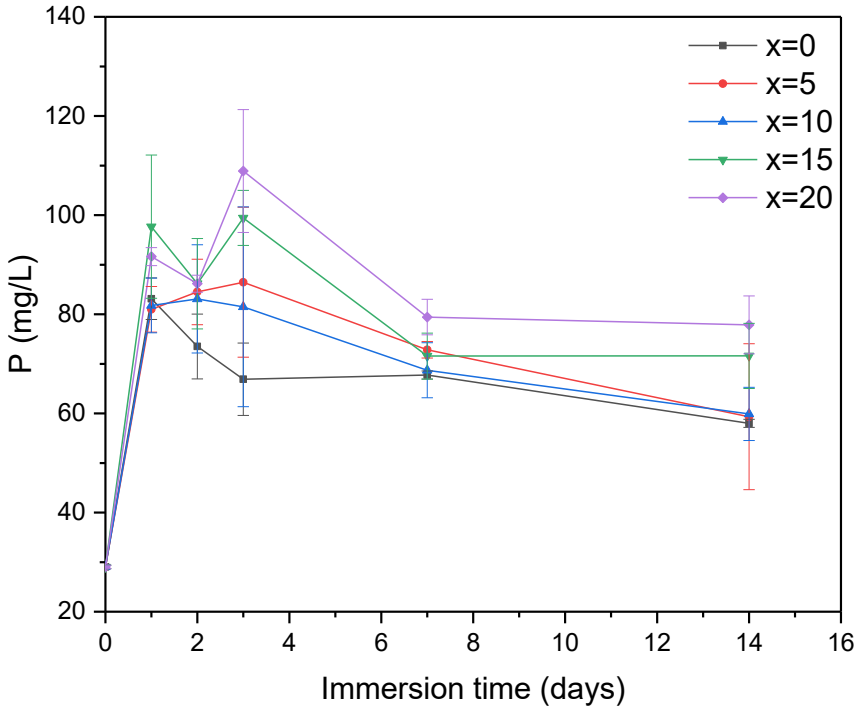
x=0
x=5
x=10
x=15
x=20
P (mg/L)
Immersion time (days)
20
40
60
80
100
120
140
0
2
4
6
8
10
12
14
16

(e)

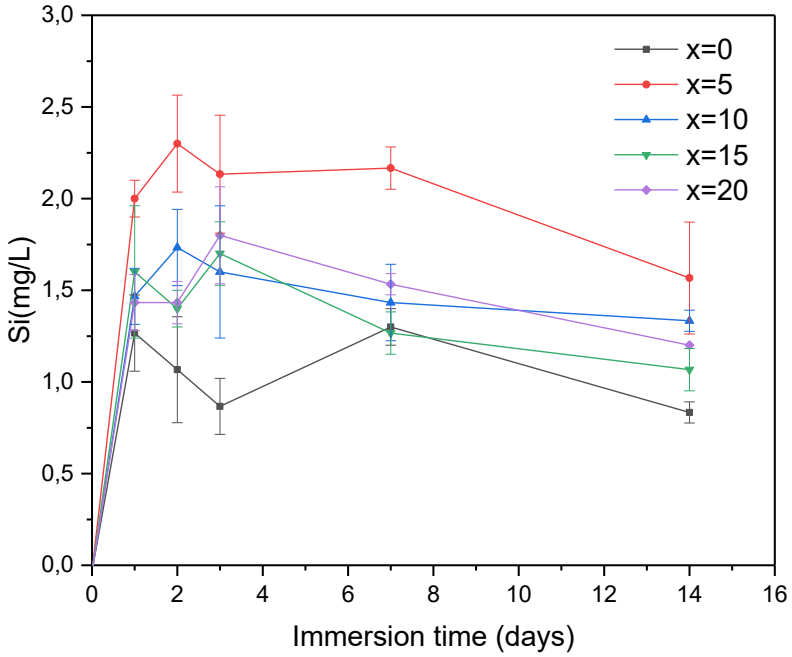

(f)

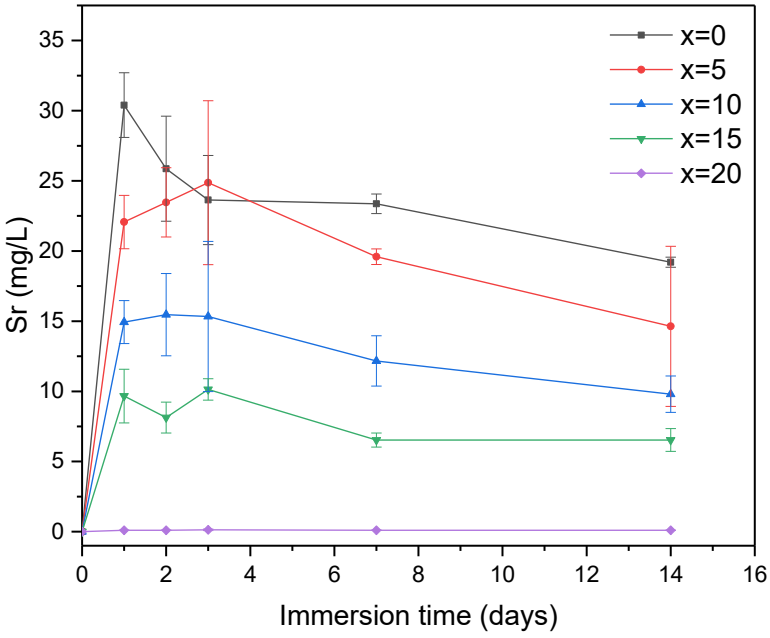

Figure 11. *Concentration of (a) B, (b) Ca, (c) Mg, (d) P, (e) Si, (f) Sr ions in SBF as a function of immersion time of <38μm particle size glasses.*

(a)

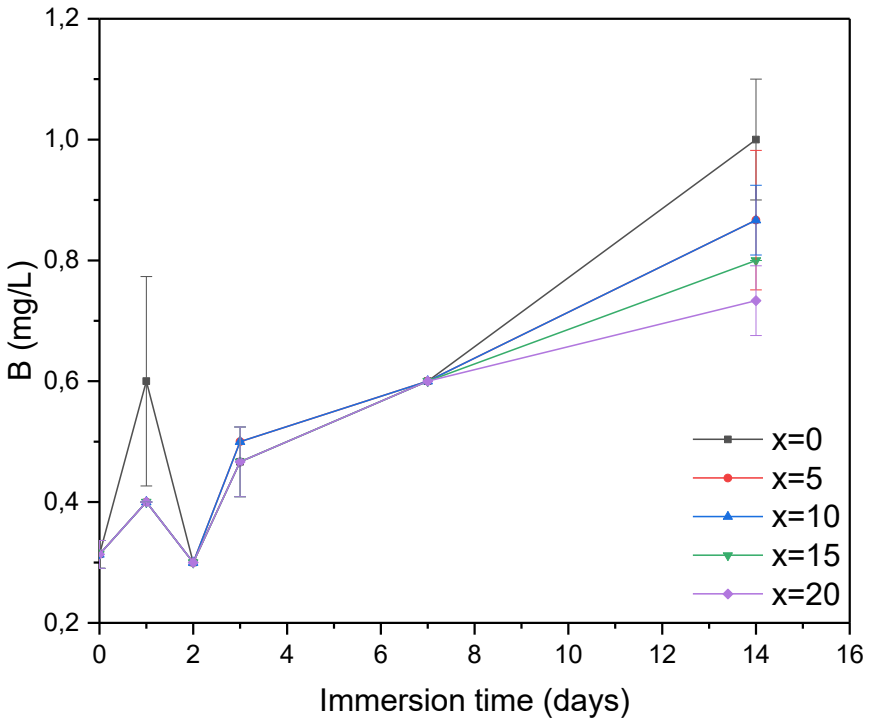
1,2
1,0
0,8
0,6
0,4
0,2
B (mg/L)
0
2
4
6
8
10
12
14
16
Immersion time (days)
x=0
x=5
x=10
x=15
x=20

(b)

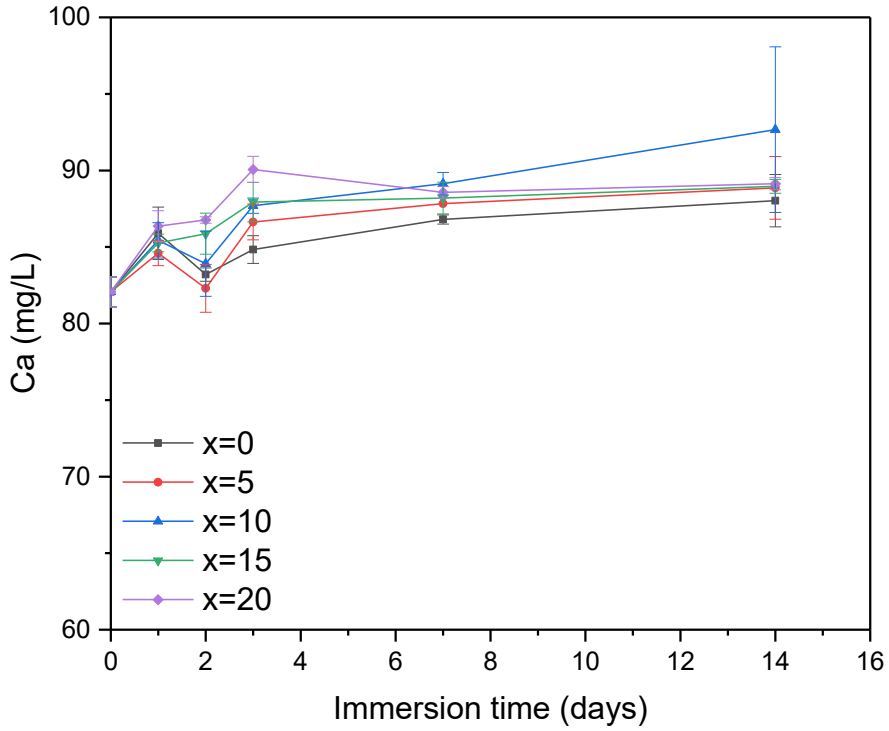
100
90
80
70
60
Ca (mg/L)
0
2
4
6
8
10
12
14
16
Immersion time (days)
x=0
x=5
x=10
x=15
x=20

(c)

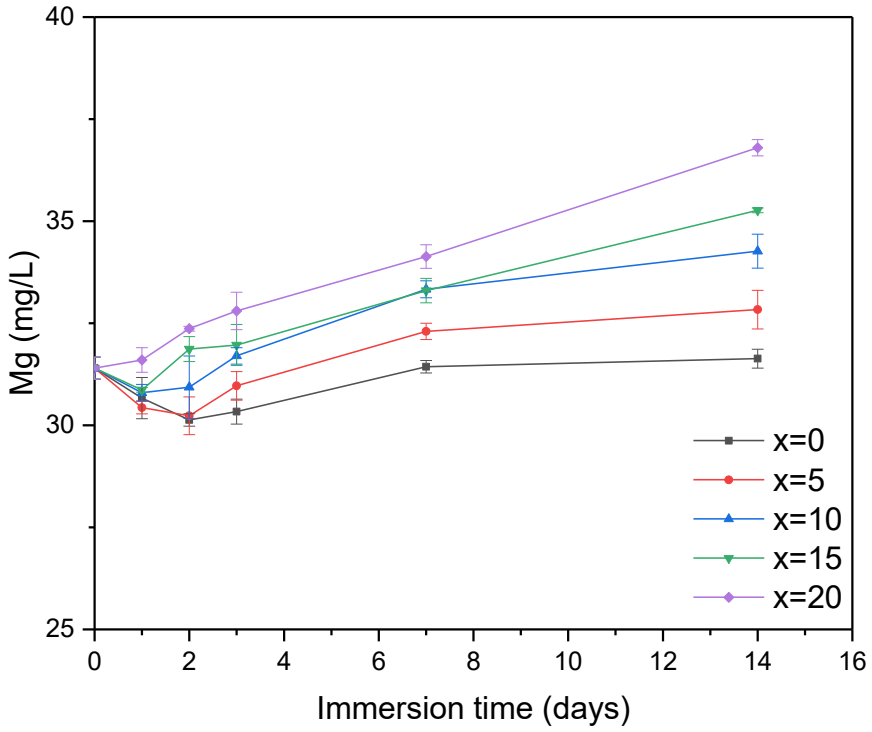
Mg (mg/L)
Immersion time (days)
x=0
x=5
x=10
x=15
x=20

(d)

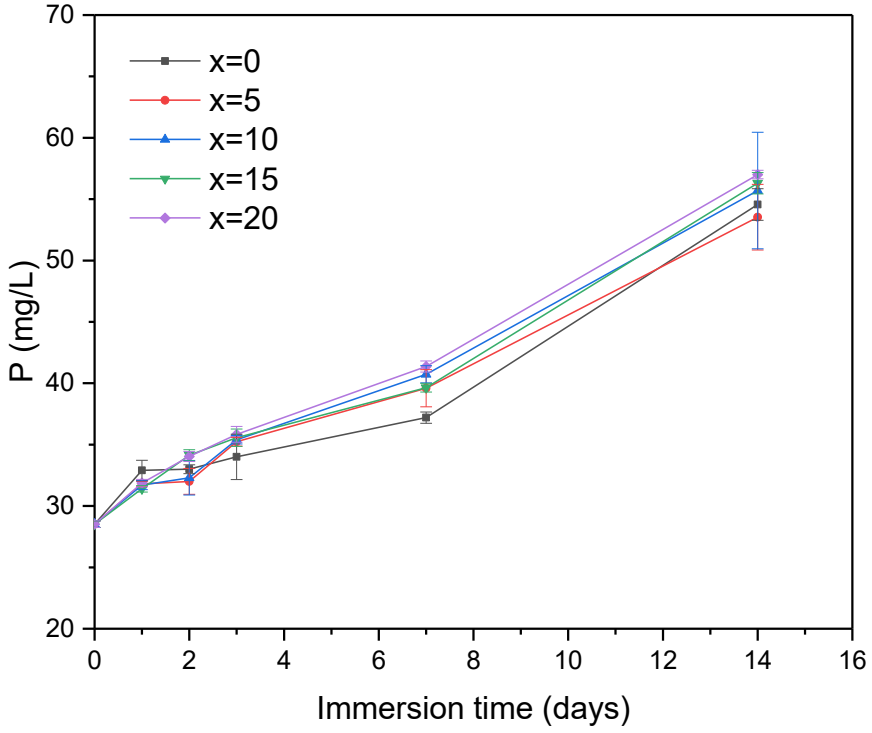
P (mg/L)
Immersion time (days)
x=0
x=5
x=10
x=15
x=20

(e)

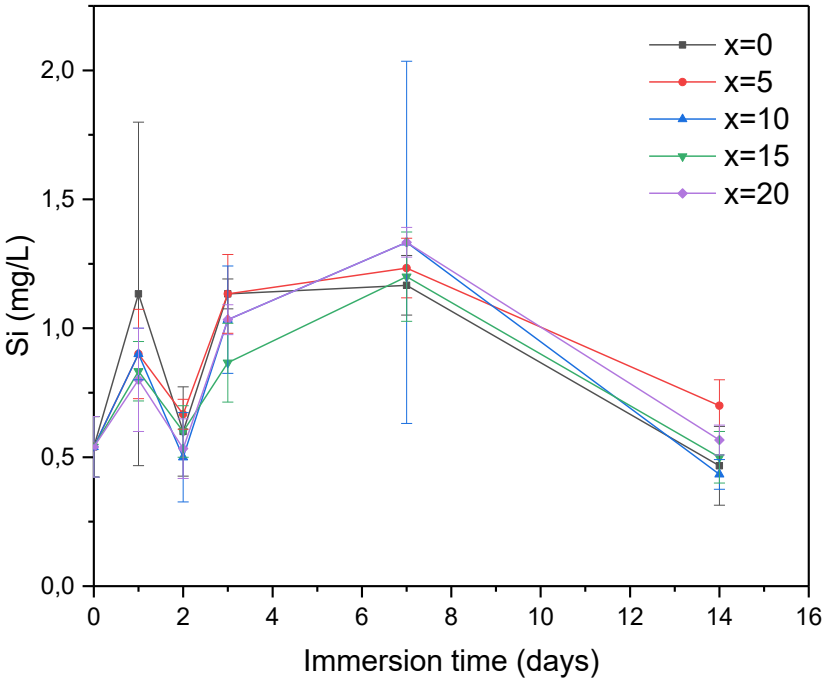

(f)

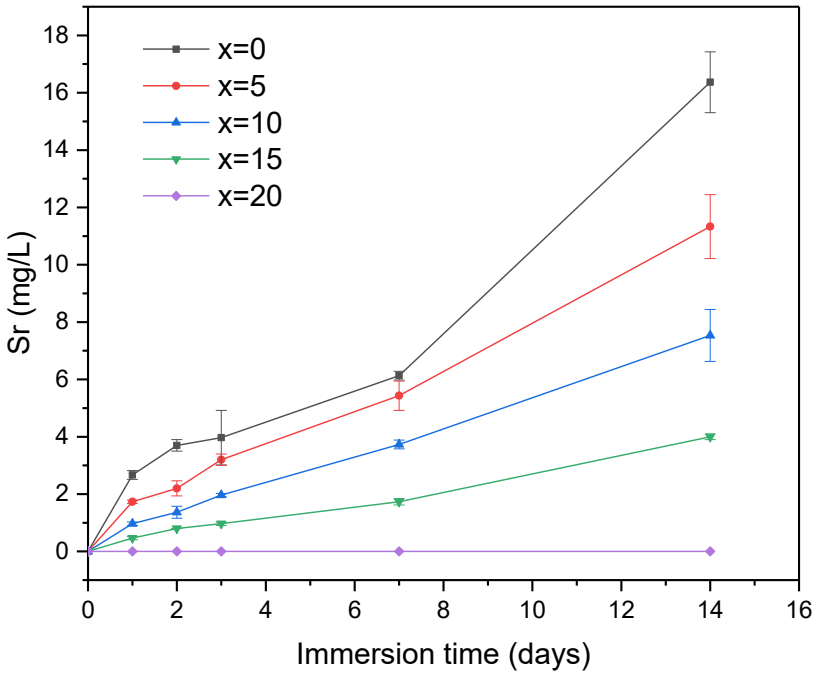

Figure 12. *Concentration of (a) B, (b) Ca, (c) Mg, (d) P, (e) Si, (f) Sr ions in SBF as a function of immersion time of 125-250μm particle size glasses.*

Figure 11 and 12 present ion release behaviour of the glasses (x = 0, 5, 10, 15, 20) with both particle sizes i.e. <38μm and 125-250μm in SBF recovered after immersion and assessed by ICP-OES. In Figure 11, it can be observed that the release of some ions (B, P, Ca, Mg) is higher with increasing the MgO concentration. In the case of Si, it appears that its release does not follow the MgO for SrO substitution. Finally, the Sr release decrease with substitution, as expected from the decreasing concentration of Sr. It is noteworthy that all ions release over 1 day of immersion and then the ion concentration remain fairly constant, indicating that the dissolution process of such small particles is rapid.

The glasses with particle size 125-250μm released ions (B, Mg, P and Sr) linearly for up to 14 days. The only exceptions are for Ca and Si ions, which only released for 1 and 3 days, respectively. The saturation of the ions release curve may be credited to the SBF solution becoming saturated with ions released from the glasses that eventually lead to the precipitation of a surface layer (Mishra, 2019).

Usually, Interpreting Ca ion release is challenging. Typically, when bioactive glasses are immersed, the Ca concentration in the SBF first increases then either decreases or remain constant. Such phenomena are seen in the parallel of decrease in the concentration of P ion with respect to immersion time. This behaviour can be the indication of Ca-P precipitation on the surface of the material (Massera & Hupa, 2014).

MgO effect on glass bioactivity depends on the MgO content in the glass and also glass overall composition due to the predominant intermediate nature of MgO. Similarly, in one study, addition of the MgO in the phosphate bioactive glasses didn't facilitate the formation of apatite layer but led to the amorphous calcium phosphate (ACP) deposition on the surface of the glasses which has been stated as a precursor phase towards formation of hydroxyapatite (Islam, et al., 2017).

Glass particle sizes have a role in the dissolution of the glass in SBF. Dissolution rate increases with the decrease in particle size and thus dissolution rate can be controlled by varying the particle size (Sepulveda, et al., 2002; Sepulveda, et al., 2000). This behaviour can be evidenced in Figure 11 and 12, where particle size less than 38μm leached ions faster than the particle size 125-250μm.

(a)

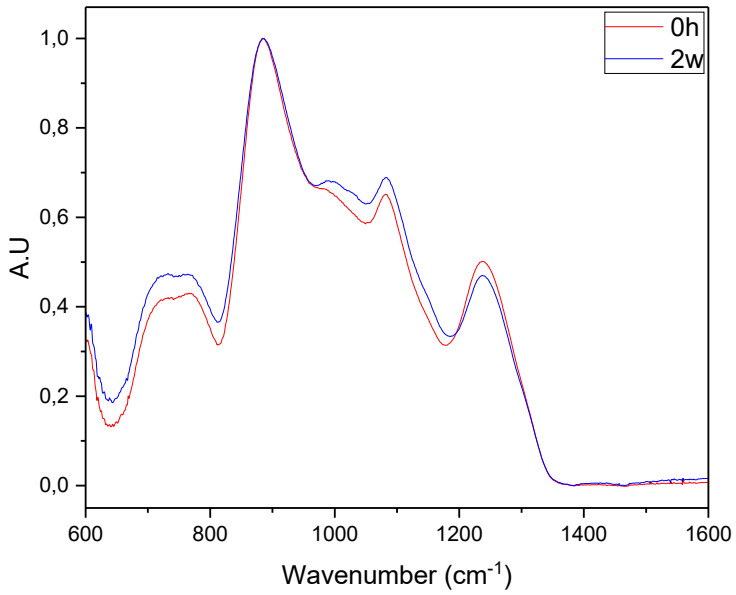

(b)

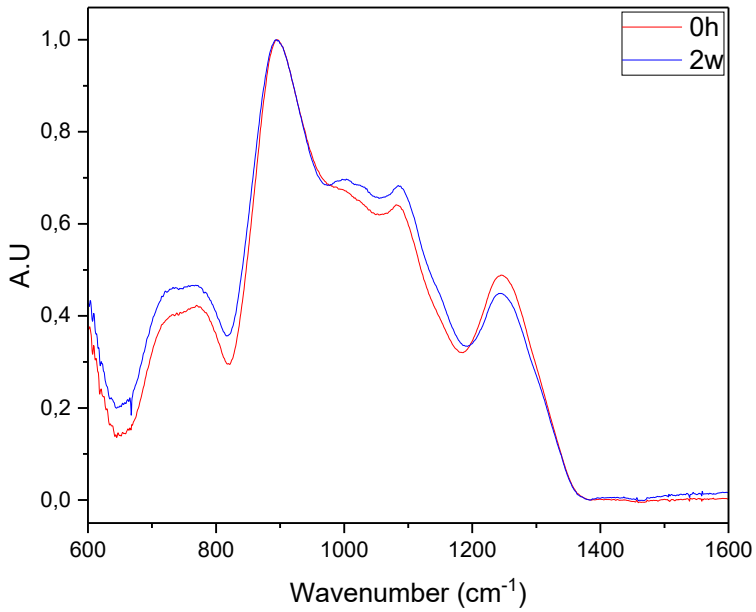

Figure 13. *FTIR spectra of the glasses (a) x=0 and (b) x = 20 with particle size <38μm after soaking in SBF for 0h and 2 weeks.*

After the *In vitro* dissolution study, FTIR was conducted on the glass powders with <38μm particle size recovered after the immersion in the SBF for the longest time point i.e. 2

weeks. For the FTIR analysis, powders with <38μm particle size was selected due to their further usability for scaffold fabrication and 2 weeks time point was chosen to see if reactive layer is formed.

Figure 13 (a) and (b) show the difference in structural changes between x = 0 and 20 glasses at 0 and 2 weeks immersion time in SBF. It can be seen from both spectra that no significant changes occurred in both investigated compositions due to the addition of MgO in the glass. However, intensities of the bands have increased at around 718, 775 and 1080 cm^{-1} whereas, intensity decreased at around 1240 cm^{-1} as a function of immersion time in both glasses. One can also observe a band formation in place of shoulders at ~1000 and ~1027 cm^{-1} with uplifted intensity in x = 20 (Figure 13 (b)) after 2 weeks of immersion time.

The decrease in intensity of band at 1240 cm^{-1} after 2 weeks immersion time indicates that the amount of Q^2 units decreases. Moreover, the increase in band at 1080 cm^{-1} can indicate the increase in Q^1 units (Massera, et al., 2013). These changes in the spectra can be related to the depolymerization of the glasses due to a hydration of phosphate chains (Clement, et al., 1999). The new bands appeared at ~1000 and ~1027 cm^{-1} after 2 weeks of immersion can be attributed to the CaP layer formation at the glass particles surface. Increase in intensity of the bands at 718 and 775 cm^{-1} exhibit the decrease in bond length and/or orthophosphate group formation when in contact with SBF (Massera, et al., 2013).

(a)

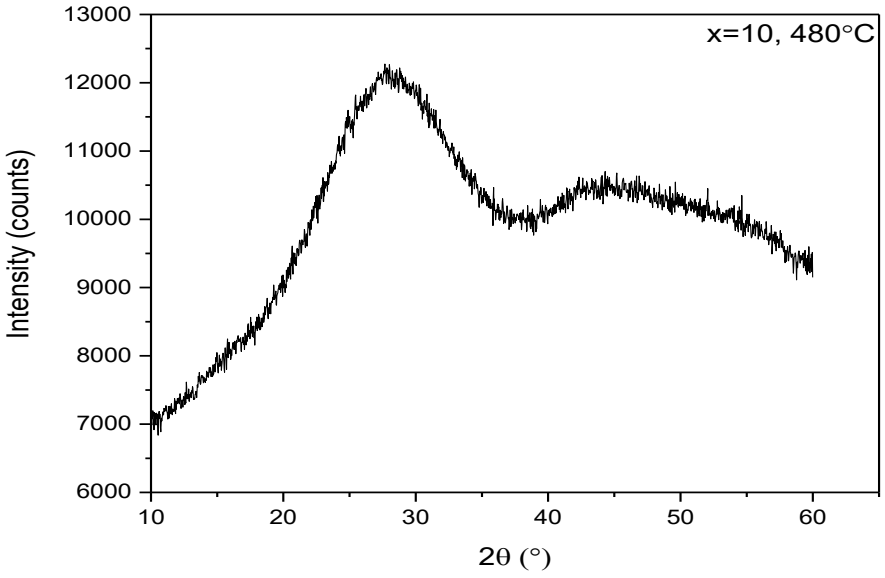

(b)

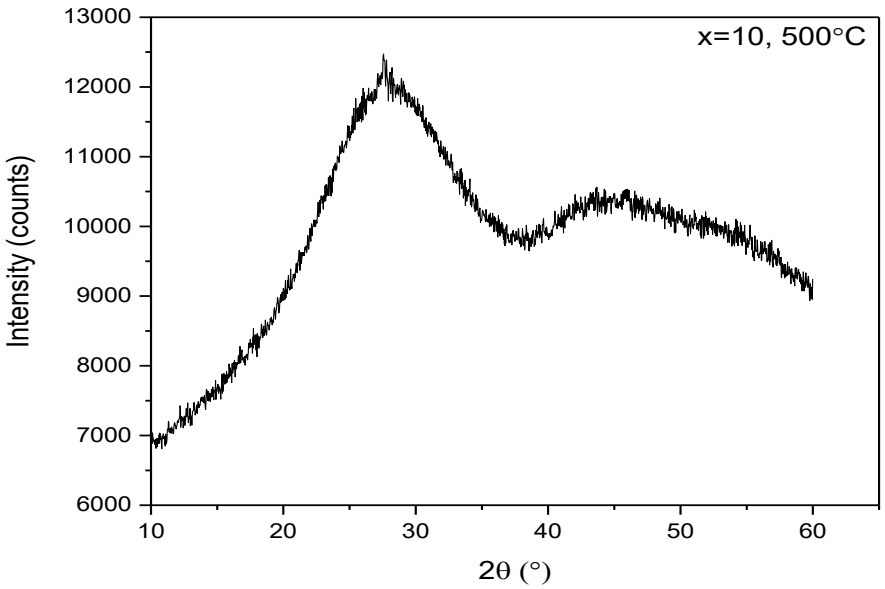

Figure 14. *XRD patterns of x = 10 glass powder sintered at (a) 480°C and (b) 500°C temperature.*

(a)

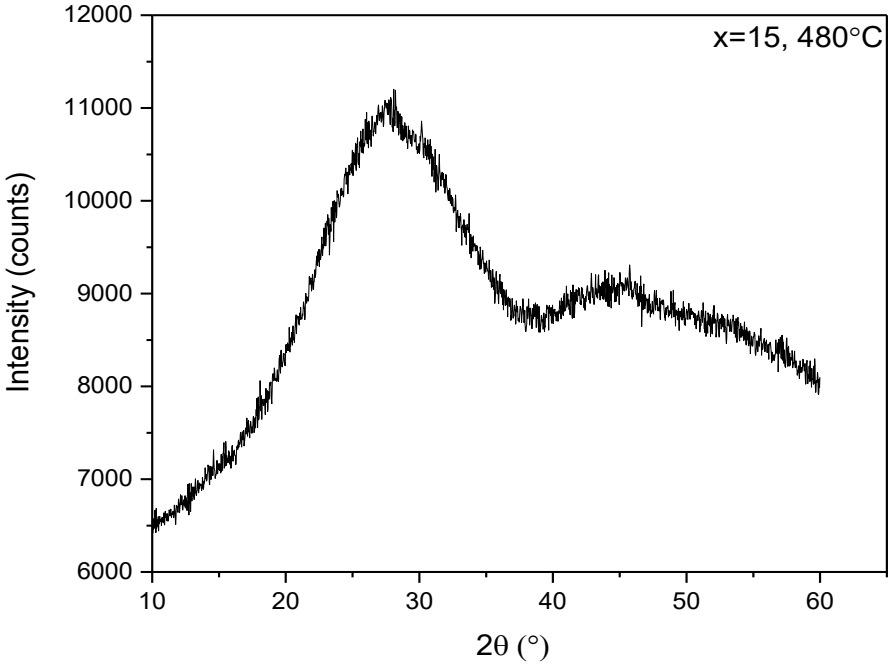

(b)

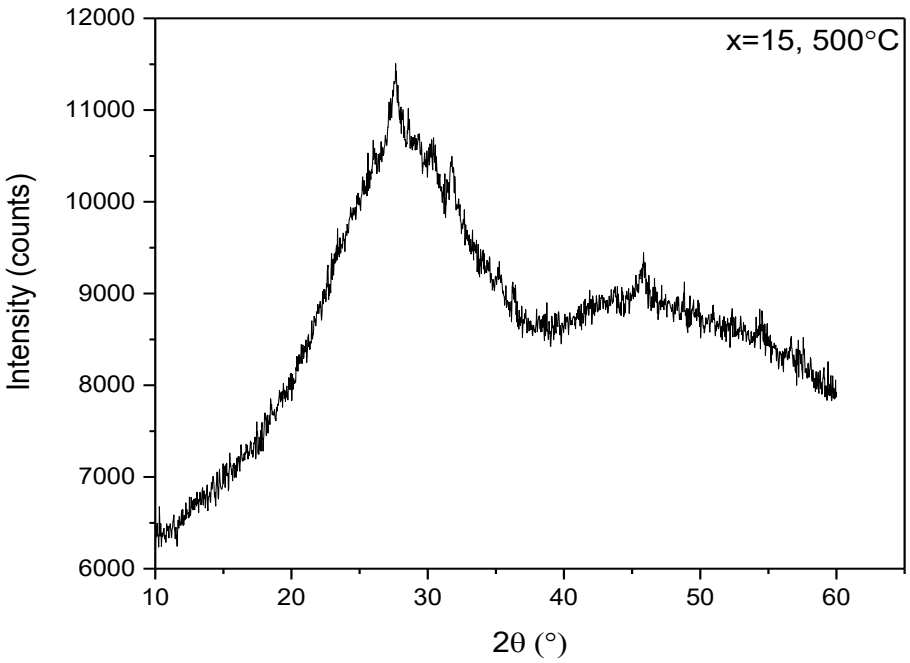

Figure 15. *XRD pattern of x = 15 glass powder sintered at (a) 480°C (b) 500°C temperature.*

After the characterization of glass powders with all the compositions, x= 10 and 15 were selected for scaffold fabrication. They have better resistance to crystallization than the glasses without the magnesium and dissolve slower than the Sr-free glasses. XRD was performed on the selected glass powders (<38μm) sintered in a pellet form at 480°C and 500°C temperature to determine the suitable temperature for the processing of scaffolds. Both Figures 14 and 15 show the diffraction patterns at (a) 480 and (b) 500 °C.

As seen from the Figure 14 (a) and 15 (a), no crystallization peaks are observed, and broad amorphous halo is formed in the range between 20° to 35° when sintered at 480°C temperature which revealed the amorphous nature of the glass. However, crystallization peaks appeared for the powders sintered at 500°C (Figure 14 (b) and 15 (b)). It is noteworthy that the x = 10 contains only one crystallization peak whereas, x = 15 shows more than one sharp peaks. It appears that, while the crystallization peak could not be seen in the DTA thermogram of x = 15, the crystallization tendency increases with increasing MgO.

4.2 Characterization of Scaffolds

Phosphate bioactive glass scaffolds with both compositions x = 10 and 15 were characterized to obtain the significant information regarding the material properties such as XRD, to confirm amorphous nature of the glass, *In-vitro* dissolution, to see ion release behaviour of the scaffolds in static condition, FTIR, to observe structural changes of the scaffolds and compression test to examine the mechanical strength of the scaffolds.

For the ink preparation, density of both glass compositions in bulk form was measured using Archimedes principle. Density of x = 10 and x = 15 were 2.78 and 2.75 ± 0.02 g/cm^{-1}, respectively. Density of the glass decreased when MgO increased in x = 15 glass, this may be because Mg has a lower molar mass which causes the density to decrease (POHJOLA, 2017).

4.2.1 XRD analysis of the Scaffolds

After the fabrication of the scaffolds through robocasting technique, all scaffolds were sintered at 490°C temperature which was thought to be the suitable temperature for scaffolds processing. Post-sintering, one scaffold from each glass composition were ground to fine powder and underwent XRD analysis.

Figure 16 (a) and (b) presents the XRD diffraction pattern of the x = 10 and x = 15 scaffolds sintered at 490°C. From the figure, it appears that despite sintering at temperature expected to be lower than the crystallization temperature, sharp peaks can be seen. It is also interesting to see that the crystallization peaks are sharper and more intense than previously reported (Figure 14 (b) and 15 (b)).

Therefore, it is conceivable that Pluronic in the ink leads to increased tendency of crystallization. Crystallization may be either due to the presence of carbons which sometimes remain in the scaffold structure even after organic binder burns off or precipitation of reactive layer during the ink process.

One can also see that the position of the sharp crystallization peaks in XRD pattern of glass powders and scaffold glass powder are not the same i.e., in glass powders, crystallization peaks are at around 27.5° whereas, in scaffolds powders, these peaks appear at around 29.6°. This can be either due to presence of carbon at the glass particles surface which modifies the primary crystal field or remnant of impurities from the ink decomposition at the glass surface.

(a)

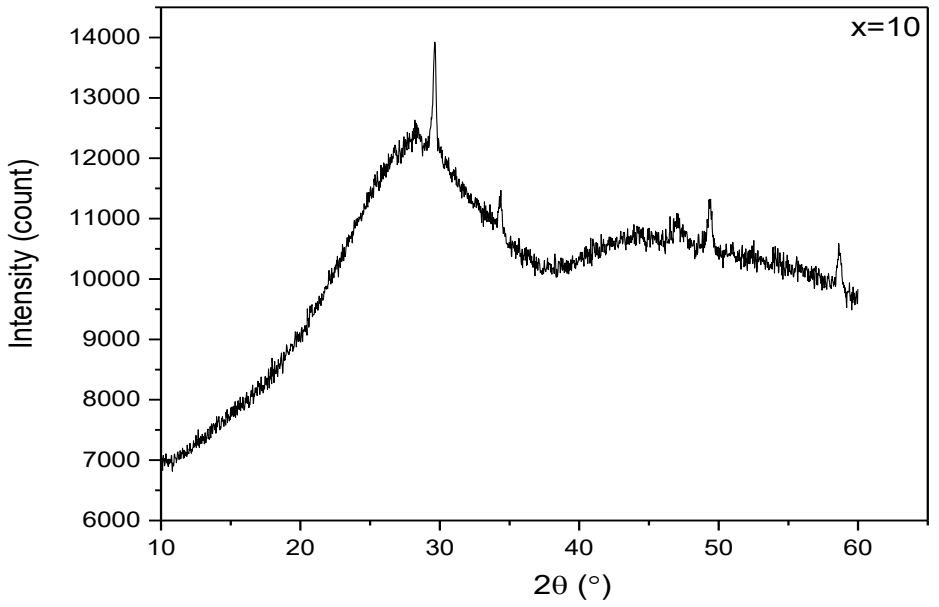

(b)

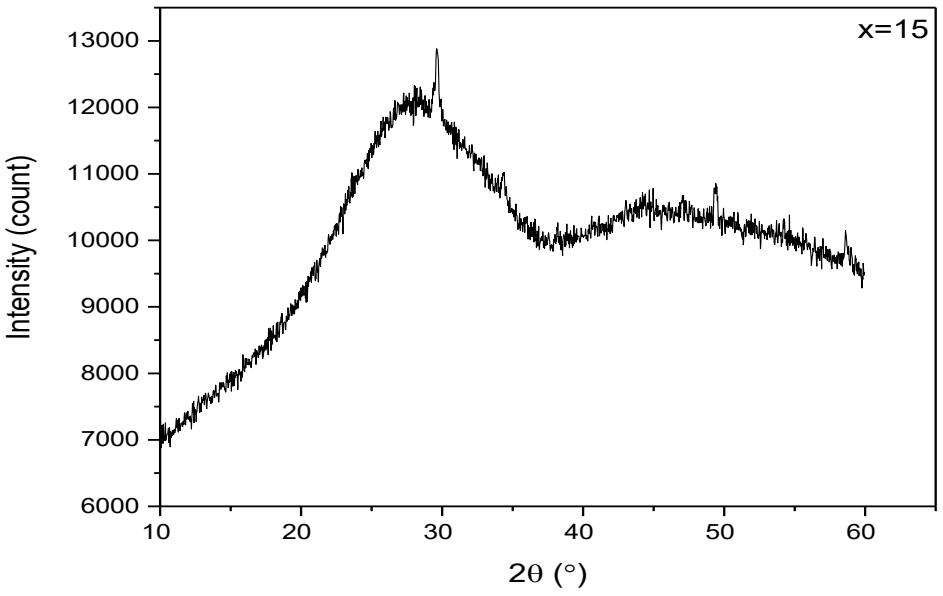

Figure 16. *XRD diffraction patterns of the robocasted scaffolds of (a) x =10 and (b) x = 15 glass compositions*

4.2.2 *In-vitro* Dissolution of Scaffolds

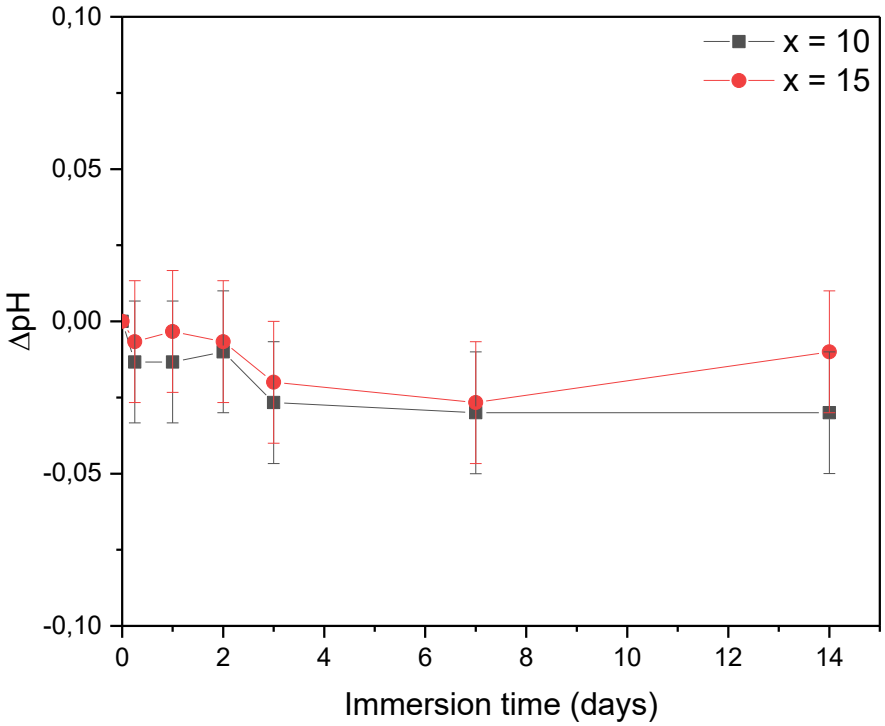

Figure 17. *Change in pH of the SBF upon immersion of scaffolds as function of immersion time.*

The *in-vitro* dissolution properties of the robocasted scaffolds were examined by immersing them in the SBF from 6 hours to 14 days. After each time point, pH of the SBF was measured and the change in pH, ΔpH, as a function of immersion time is presented in Figure 17, respectively. It can be seen that no significant change occurred in the pH within the accuracy of measurement for the whole immersion period. Hence, solution remained at a physiological pH.

(a)

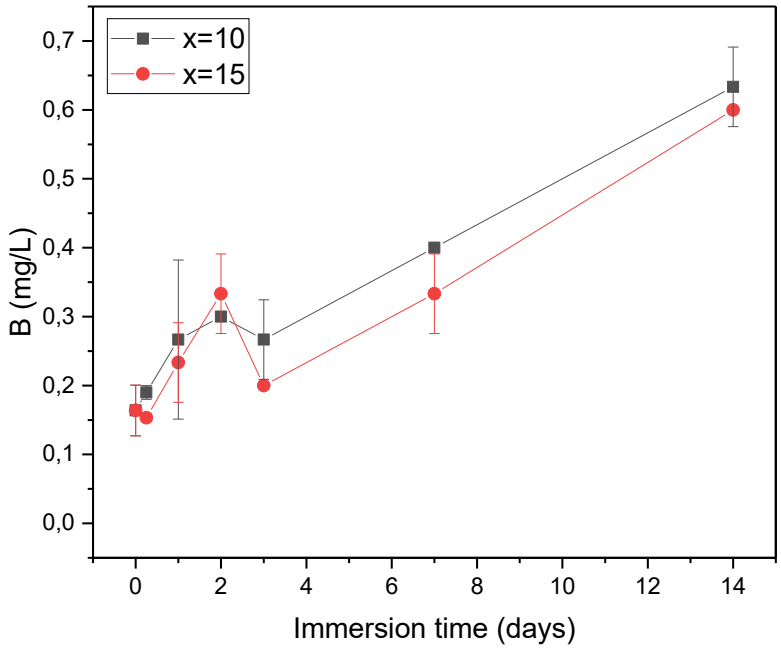
x=10
x=15
B (mg/L)
0,0
0,1
0,2
0,3
0,4
0,5
0,6
0,7
0
2
4
6
8
10
12
14
Immersion time (days)

(b)

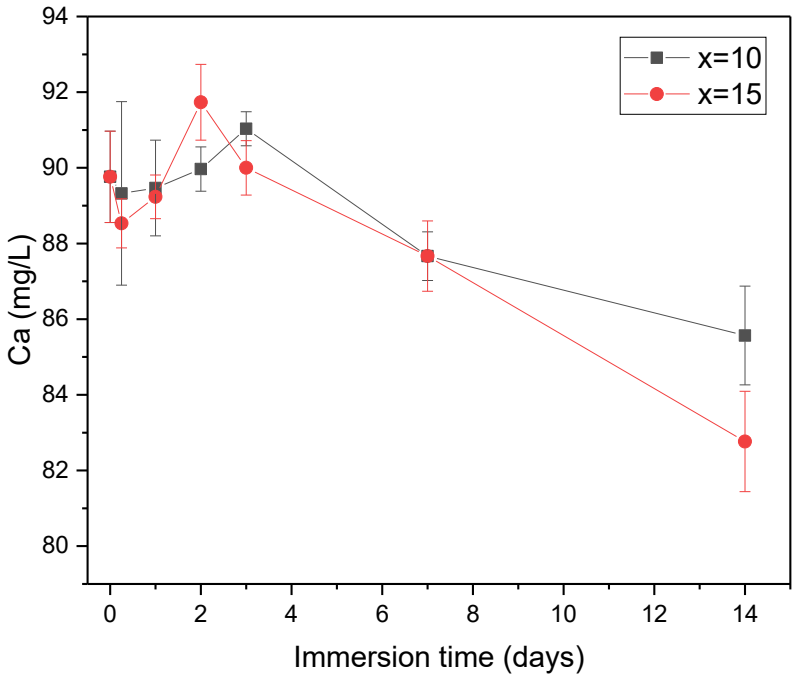
x=10
x=15
Ca (mg/L)
80
82
84
86
88
90
92
94
0
2
4
6
8
10
12
14
Immersion time (days)

(c)

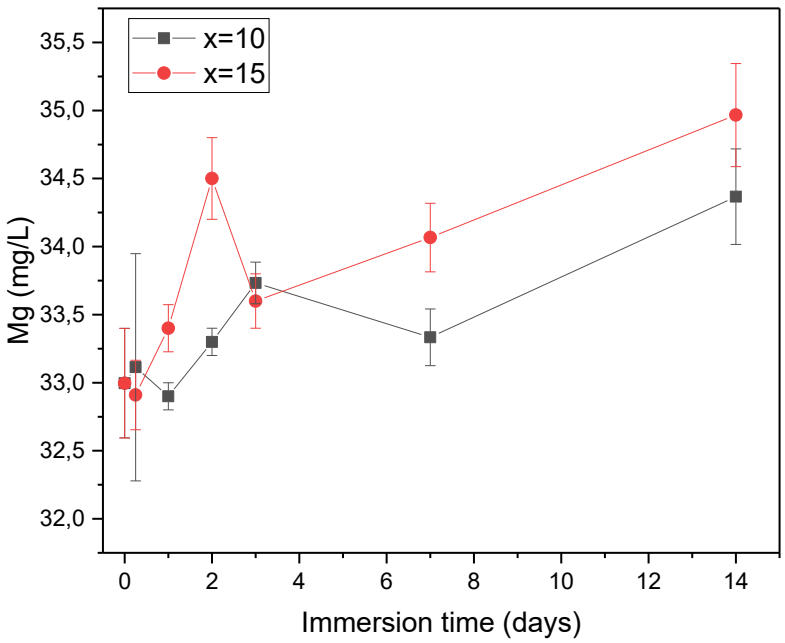
x=10
x=15
Mg (mg/L)
35,5
35,0
34,5
34,0
33,5
33,0
32,5
32,0
0
2
4
6
8
10
12
14
Immersion time (days)

(d)

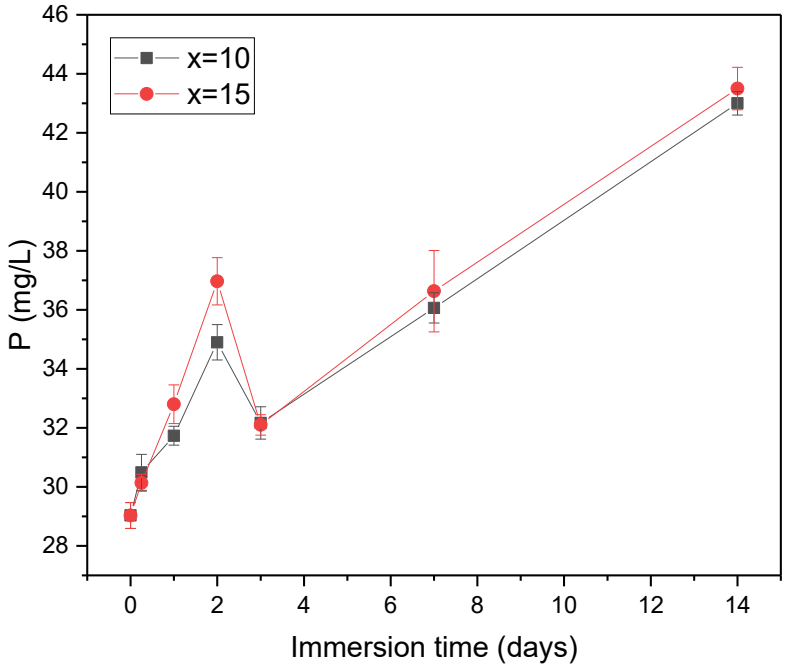
x=10
x=15
P (mg/L)
46
44
42
40
38
36
34
32
30
28
0
2
4
6
8
10
12
14
Immersion time (days)

(e)

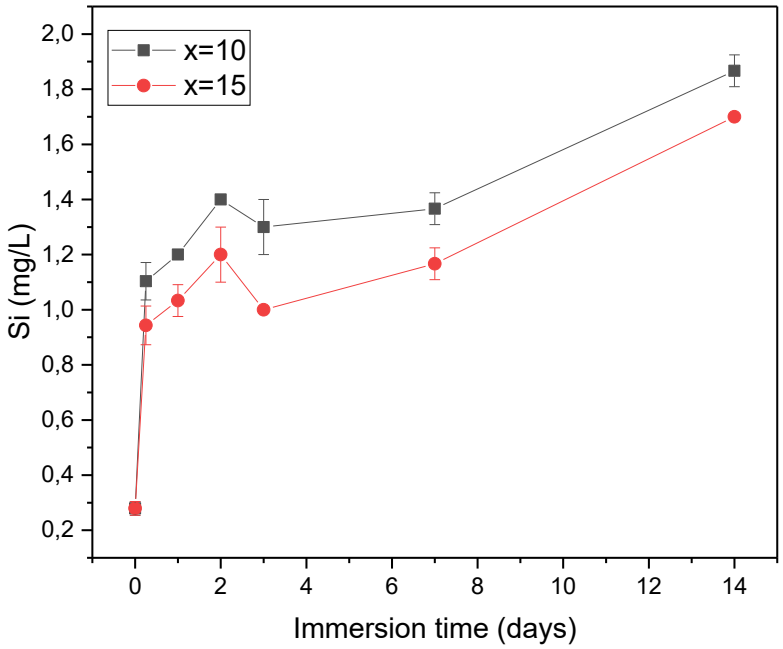

(f)

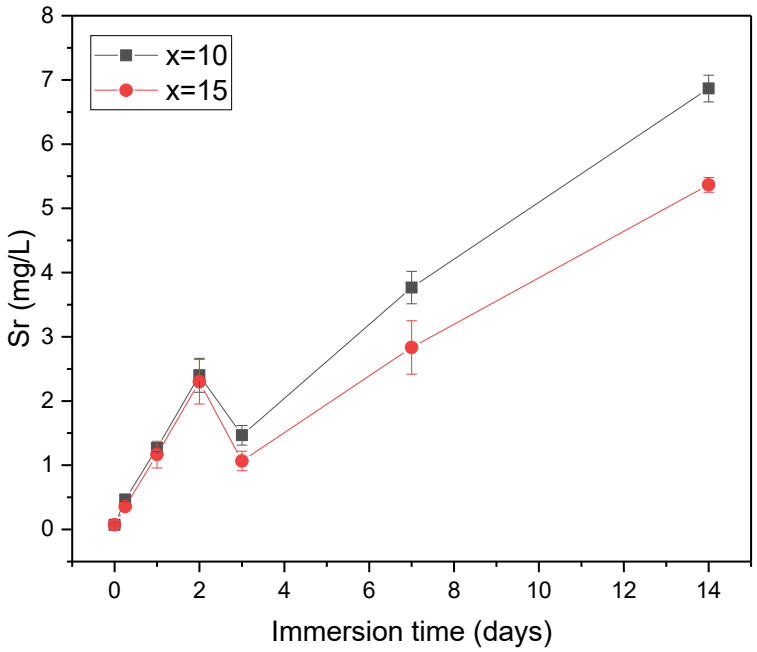

Figure 18. *Ion release behavior of the scaffolds containing (a) B, (b) Ca, (c) Mg, (d) P, (e) Si, (f) Sr elements in the SBF as a function of immersion time.*

The rate of biodegradation of bioactive material is complex but plays an important role in its stability after implantation. In vitro dissolution study is considered helpful to understand the soluble nature of prepared glass, especially in SBF solution where its ions affect the network by exchanging ions produced from the glass in the SBF (Gurusamy, et al., 2012). Generally, ions are released from the surface of the glass during the bioactivity mechanism; therefore, additional information can be obtained during ionic concentration evaluation in the SBF during dissolution test (Bruckner, et al., 2016).

Figure 18 shows the B, Ca, Mg, P, Si and Sr ions release profile of scaffolds evaluated with ICP-OES. It can be observed in the graphs that there is a progressive release of all the ions until 14 days besides a small drop in 3 days time point for all the ions except Ca. Ca concentration was increasing linearly until 3 days for x =10 and 2 days for x = 15 followed by sudden precipitation for the rest of the testing time point. Furthermore, ion released trend of x = 15 scaffolds remained lower than x = 10 except Mg and in P, for which the release is similar. In all the graphs, one can notice that the plateau was not reached.

The decreasing concentration of Ca ion for the longer time point in the SBF indicates the consumption of Ca ion which eventually leads to the precipitation of the reactive layer. This is also in agreement with the decrease in P, Mg, and Sr assumed to be also incorporated in the reactive layer. Moreover, Ca is already present in the SBF; therefore, the solution becomes super-saturated in the early immersion time point (Massera, et al., 2013; Mishra, et al., 2016). According to the earlier studies, CaO content is important in terms of solubility behaviour of the glass and there is a correlation between MgO content and Ca ion release; therefore, when the MgO content is increased in the glass, the solubility decreases (Franks, et al., 2002).

Overall, there was not great difference observed in the ions released from the scaffolds with x = 10 where content of MgO and SrO is same and with x = 15, where MgO content is more than SrO in the glass. In both compositional scaffolds, ions were releasing progressively despites a drop in 3 days time point which can corresponds to the time at which the layer starts forming. The precipitation of the reactive layer seems to be faster and more pronounced for the x = 15 glass, as shown by the greater drop in Ca, Mg, and Sr concentration for this glass.

If these results are compared with the dissolution studies performed on the glass particles, ions released did not reach the plateau during scaffolds dissolution studies whereas, ions release became stable after 3 days of immersion. The difference can be due to the lower specific surface in scaffold compared to particles.

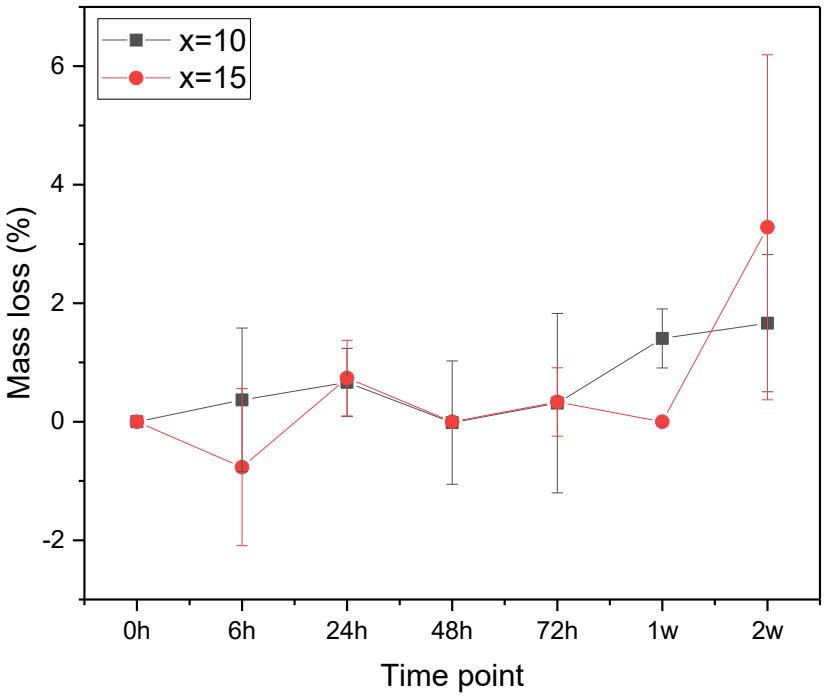

Figure 19. *Mass loss of robocasted scaffolds after immersion in SBF.*

Figure 19 shows the mass loss of both compositional scaffolds after each time point in the SBF. It can be seen that the mass loss of the scaffolds is between 0 to 3 % after 2 weeks of immersion time in the SBF which is negligible, scaffold with x = 15 gained mass after 6 hours time point which is due to the little SBF absorption. The mass loss result is in the agreement with the ΔpH results of the scaffolds as the pH was not changed because mass loss did not occur. This also proves that the overall dissolution of the two scaffolds are fairly similar.

4.2.3 Mechanical Property

During the development of the bioactive glass scaffolds for the structural bone loss repair, mechanical properties should be comprehensively examined because their properties change with time (Liu, et al., 2013). That is the reason that besides the most studies on mechanical properties of the bioactive glass scaffolds, focus has been on evaluating the strength and Young's modulus in compression of the as-fabricated scaffolds or scaffolds that were immersed in SBF (Fu, et al., 2011).

(a)

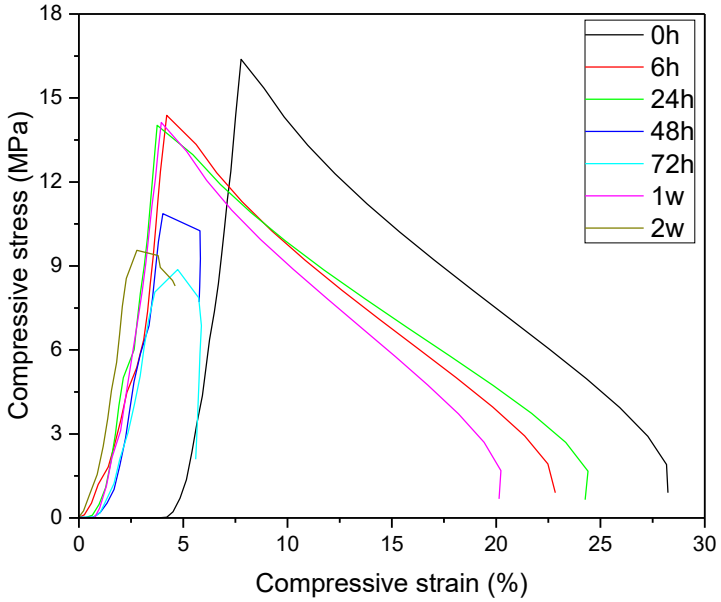

(b)

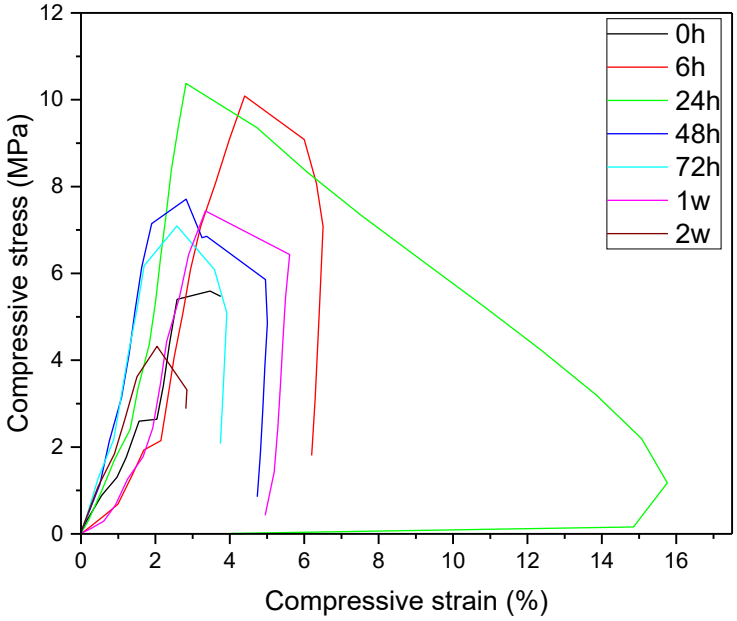

Figure 20. *Compressive stress vs. strain of (a) x =10 and (b) x = 15 glass scaffolds as a function of immersion time.*

(a)

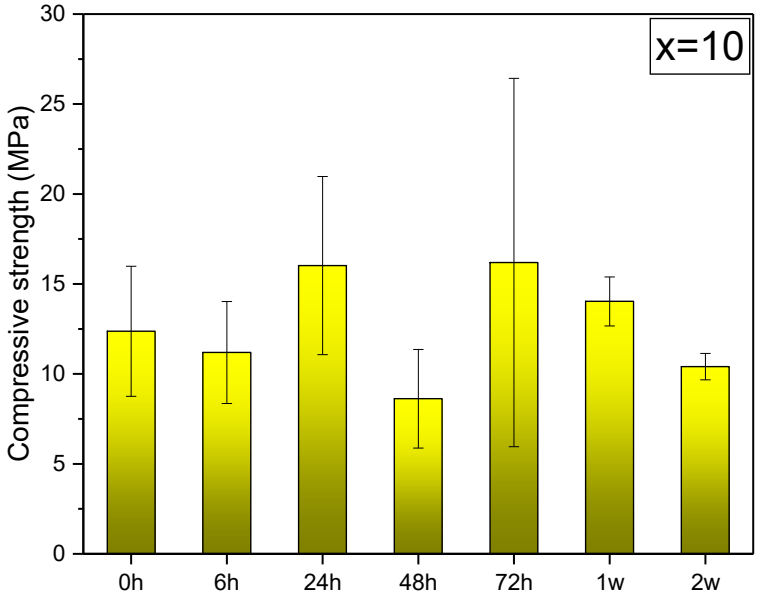

(b)

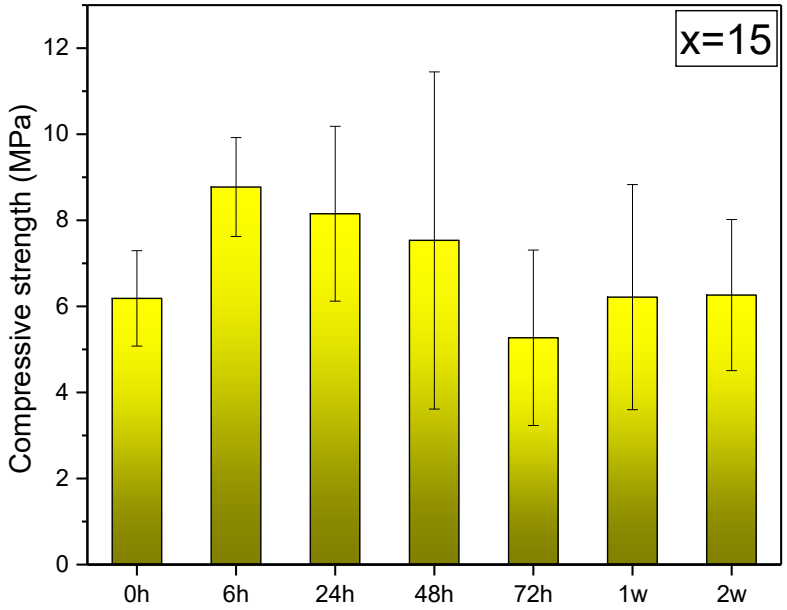

Figure 21. *Compressive strength of the (a) x =10 (b) x = 15 robocasted glass scaffolds as a function of immersion time.*

(a)

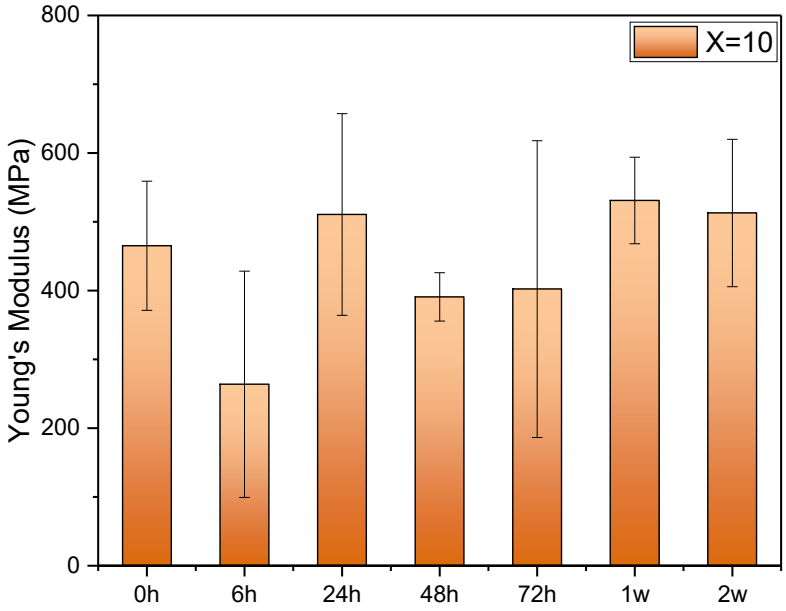

(b)

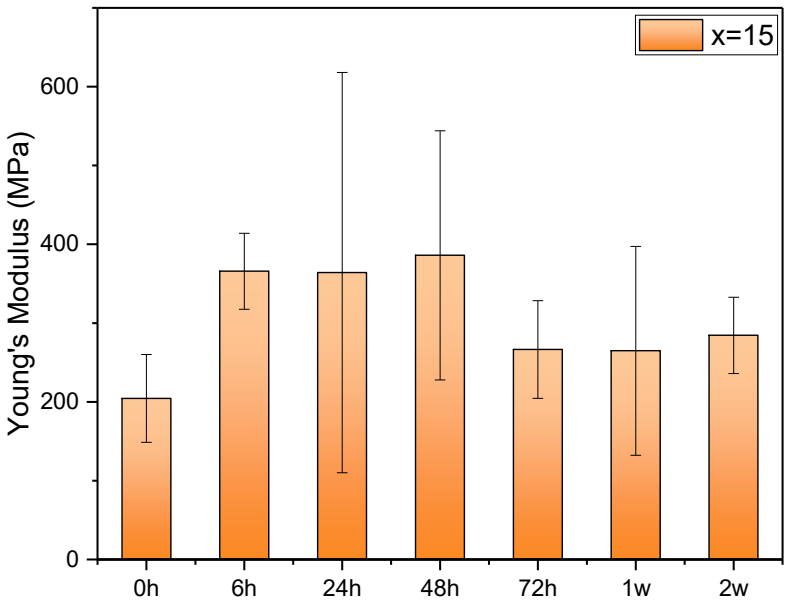

Figure 22. *Young's modulus of the (a) x =10 and (b) x = 15 glass scaffolds as a function of immersion time.*

Figure 20 presents the mechanical behaviour of the robocasted scaffolds in compression as a function of immersion time in SBF. All scaffolds compressive stresses are characteristic of a brittle material. The force rises rapidly with minimal deformation of the scaffold, until reaching fracture. The maximum force before failure can be assigned to the maximum compressive strength while the linear fit of the initial rise in force as a function of strain corresponds to the elasticity of the materials.

Compressive strengths of both compositional scaffolds were measured before and after certain immersion time point and the average ± SD obtained are shown in Figure 21. It can be seen that over the course of the immersion, the compressive strength does not significantly change and remain within 8-16MPa in the case of the scaffold x=10 and within 5-9 MPa for the scaffold x=15. The compressive strength results indicate that the glass x=10 sintered more effectively than the glass x=15.

Ideally, scaffold should act as a temporary template that mimics the function of healthy bone by facilitating new bone growth while supporting surrounding tissues when implanted on load-bearing site. Therefore, scaffold needs to show good mechanical properties after implantation and not degrade before the healing is completed (Baino, et al., 2019). The obtained values are within values reported for cancellous bone (2-12 MPa (Hench, 1991)) or even higher, indicating that up to 2 weeks, the scaffold can support the mechanical load in non-load bearing applications. Variation in the compressive strength can be reduced by optimizing the scaffold fabrication process (Baino, et al., 2019).

Young's modulus of three parallel samples of both (a) x = 10 and (b) x = 15 glass scaffolds were measured as a function of immersion time in the SBF and average ± SD were obtained and plotted which are presented in Figure 22. For both glass scaffolds, the Young's Modulus remain almost unchanged as a function of immersion time in SBF. The Young's modulus of x = 10 and x = 15 glass scaffolds before immersion was 465 ± 94 MPa and 204 ± 56 MPa and after 2 weeks immersion time was 513 ± 107 and 284 ± 48 MPa, respectively. It is true for the scaffolds that the porosity of the porous material mainly determines the Young's modulus of the material (Jian, et al., 2015).

The modulus obtained from the scaffolds were in the range between 460 – 515 and 200 to 290 MPa for x = 10 and x = 15 glass scaffolds which exist in the range of values reported for trabecular bone (100 – 5000 MPa (Fu, et al., 2011)), respectively. It is difficult to calculate the absolute values of the Young's modulus from the compression tests due to the scaffolds geometry and large deformation. However, linear fit of the data up to the elastic limit can be used to calculate modulus.

4.2.4 Structural Properties

Structural analysis was carried out of the fabricated scaffolds to obtain the information regarding changes on the surface of the glasses after immersion in SBF. Spectra were normalized to the band having highest intensity.

Figure 23 presents the FTIR spectra of (a) x = 10 and (b) x = 15 glass scaffolds fabricated using robocasting technique and immersed in SBF for 0h and 2w time points. Scaffolds were ground to fine powder and underwent FTIR spectroscopy.

(a)

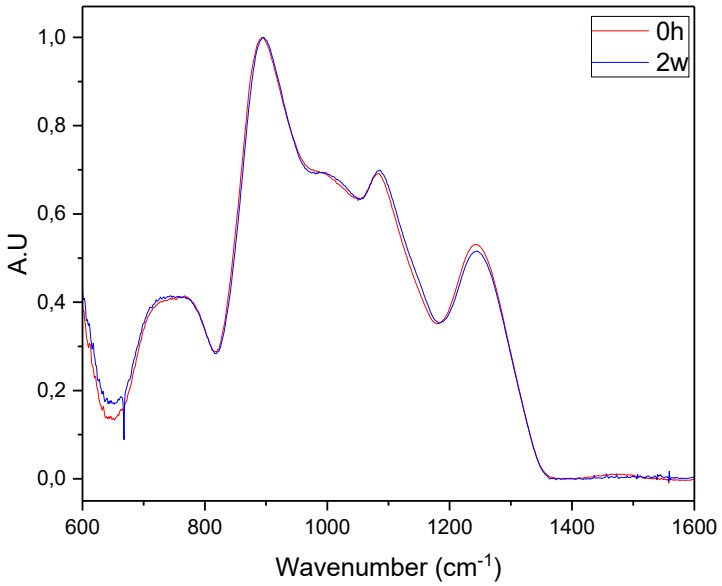

(b)

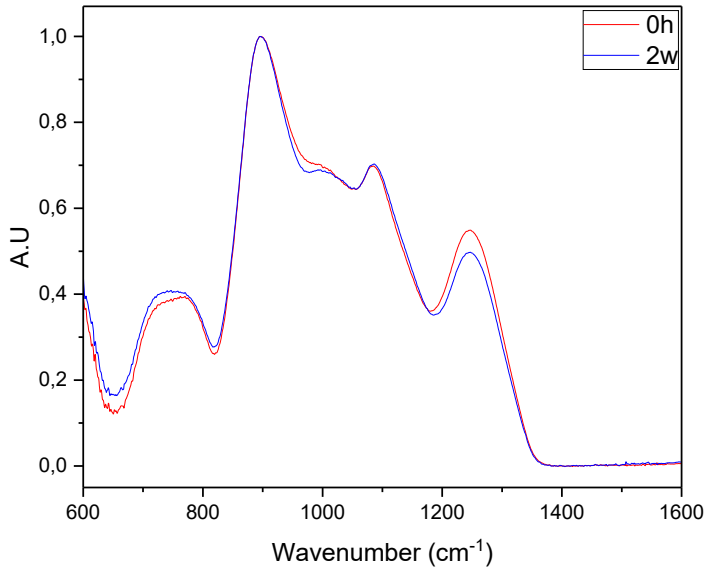

Figure 23. *FTIR spectra of (a) x = 10 and (b) x = 15 glass scaffolds obtained after 0 and 2 weeks immersion time point in SBF.*

FTIR analysis of the scaffolds revealed that no significant change occurred to the structure of the scaffolds glass surface. Similar to the glass powder FTIR results before robocasting, It was observed that in x = 15, the intensity of the band was decreased after 2 weeks immersion time at ~1240 cm^{-1} which indicates the decreasing of network connectivity and increasing Q^1 units (Mishra, et al., 2016) due to the glass is in contact with SBF. A new band peaking with small intensity at ~1000 cm^{-1} which can be attributed to the PO^- in Q^0 units and could be assigned to CaP layer formation (Massera, et al., 2013). Whereas, there was no effect of immersion time and MgO content on the structure of the band in scaffold with x = 10 glass. Unlike the intensity increased at ~1080 cm^{-1} in glass powder structure, here it is same in both compositions. Shifting of the bands towards higher wavenumber is also in the agreement with the results of glass powder FTIR before robocasting. The decrease in intensity of band in x = 15 at 1240 cm^{-1} after 2 weeks of immersion directs the decrease in density of PO bonds with the addition of MgO (G., et al., 2012).

By these results, one can say that, sintering and *in-vitro* dissolution of the robocasted scaffolds even after two weeks did not bring any major change in the structure than the glass structure before scaffolds fabrication.

5. CONCLUSION

In this thesis work, five compositions of phosphate bioactive glass were prepared. In each composition, MgO was increased at the expense of SrO with the aim to investigate the thermal and bioactive properties of the glasses. Amongst all, two suitable glass compositions were selected for scaffolds fabrication using robocasting technique, followed by their *in-vitro* characterization.

With an increase in MgO content in the glass, T_g and T_p were increased linearly except x = 15 and 20 where, T_p disappeared eventually. Surprisingly, T_x was not changed much which ultimately leads to constant ΔT. Ion release behaviour in <38μm particle size was higher than 125-250μm particle size in all glass compositions. Additionally, in <38μm particle size, after 1 day, ions release became constant. This suggests that ion dissolution is dependent on the particle size. FTIR result revealed a new band with low intensity on x = 20 glass structure after two weeks of immersion in SBF, which indicated the CaP layer formation.

After sintering x = 10 and 15 glass powders at different temperatures, 490°C was considered to be the suitable sintering temperature for robocasted x = 10 and 15 glass scaffolds in order to prevent crystallization in the glass. After scaffolds were sintered, unexpected sharp crystallization peaks were observed through XRD. These peaks were assumed to be due to the carbon left from the binder in the scaffold structure during sintering which might favoured crystallization of the glass. pH of the SBF remained unchanged over the course of 2 weeks. Continuous ions release was observed in scaffolds with both compositions for 2 weeks immersion in SBF, except there was the drop of ion release in 2 days time point which indicated the CaP layer formation. This result was evidenced from the FTIR result where new band was formed due to the formation of CaP layer, otherwise FTIR revealed no major change in the structure of the scaffold glass even after 2 weeks immersion in SBF. Mechanical strengths of x = 10 and 15 glass scaffolds were within the range of cancellous bone. Thus, these scaffolds could be useful in non-load bearing applications.

To sum up, SrO replacement by MgO seems an effective way to enhance thermal properties as well as bioactive properties of the glasses. Robocasted scaffolds showed good mechanical strength for application in non-load bearing applications. In future, more comprehensive analysis of the MgO effects could be done to gain further understanding.

REFERENCES

Ahmed, I. y otros, 2004c. Processing, characterisation and biocompatibility of iron-phosphate glass fibres for tissue engineering. *Biomaterials,* 25(16), pp. 3223-3232.

Ahmed, I., Lewis, M., Olsen, I. & Knowles, J. C., 2004a. Phosphate glasses for tissue engineering: Part 1. Processing and characterisation of a ternary-based P2O5-CaO-Na2O glass system.. *Biomaterials,* 25(3), pp. 491-9.

Ahmed, I., Lewis, M., Olsen, I. & Knowles, J. C., 2004b. Phosphate glasses for tissue engineering: Part 2. Processing and characterisation of a ternary-based P2O5–CaO–Na2O glass fibre system. *Biomaterials,* 25(3), pp. 501-507.

Aitasalo, K., Kinnunen, I., Palmgren, J. & Varpula, M., 2001. Repair of Orbital Floor Fractures With Bioactive Glass Implants. *Journal of Oral Maxillofacial Surgery,* 59(12), pp. 1390-1395.

Al-Qaysi, M., 2018. *Development of Phosphate Based Glass Scaffolds for the Repair of Craniofacial Bone,* London: University College London.

Amini, A. R., Laurencin, C. T. & Nukavarapu, S. P., 2012. Bone Tissue Engineering: Recent Advances and Challenges. *PubMed Central,* 40(5), pp. 363-408.

Baino, F. y otros, 2019. Robocasting of Bioactive SiO2-P2O5-CaO-MgO-Na2O-K2O. *Journal of Healthcare Engineering,* p. 12.

Bardsley, K. y otros, 2017. Repair of bone defects in vivo using tissue engineered hypertrophic cartilage grafts produced from nasal chondrocytes. *Biomaterials,* Volumen 112, pp. 313-323.

Basha, R. Y., T.S., S. K. & Doble, M., 2015. Design of biocomposite materials for bone tissue regeneration. *Materials Science and Engineering: C,* Volumen 57, pp. 452-463.

Ben-Nissan, B., 2003. Natural bioceramics: from coral to bone and beyond. *Current Opinion in Solid State and Materials Science,* 7(4-5), pp. 283-288.

Bhushan, M. y otros, 2015. Bioactive Materials: A Short Review. *Journal of Orofacial Research,* 5(4), pp. 138-141.

Biga, L. M. y otros, 2019. *Anatomy & Physiology - (Bone Tissue and the Skeletal System).* Oregon: Open Oregon State.

Bose, S., Vahabzadeh, S. & Bandyopadhyay, A., 2013. Bone tissue engineering using 3D printing. *Materialstoday,* 16(12), pp. 496-504.

Brovarone, C. V., Vern´, E. & Appendino, P., 2006. Macroporous bioactive glass-ceramic scaffolds. *Journal of Materials Science: Materials in Medicine,* 17(11), p. 1069–1078.

Brow, R. K., 2000. Review: the structure of simple phosphate glasses. *Journal of Non-Crystalline Solids,* Volumen 263-264, pp. 1-28.

Brow, R. K. & Tallant, D. R., 1997. Structural design of sealing glasses. *Journal of Non-Crystalline Solids,* Volumen 222, pp. 396-406.

Bruckner, R., Tylkowski, M., Hupa, L. & Brauer, D. S., 2016. Controlling the ion release from mixed alkali bioactive glasses by varying modifier ionic radii and molar volume. *Journal of Materials Chemistry B,* 4(18), pp. 3121-3134.

Bunker, B. C., Arnold, G. W. & Wilder, J. A., 1984. Phosphate glass dissolution in aqueous solutions. *Journal of Non-Crystalline Solids,* 64(3), pp. 291-316.

Carta, D. y otros, 2007. A structural study of sol–gel and melt-quenched phosphate-based glasses. *Journal of Non-Crystalline Solids ,* 353(18-21), pp. 1759-1765.

Chatzistavrou, X. y otros, 2006. INFLUENCE OF PARTICLE SIZE ON THE CRYSTALLIZATION PROCESS AND THE BIOACTIVE BEHAVIOR OF A BIOACTIVE GLASS SYSTEM. *Journal of Thermal Analysis and Calorimetry,* 85(2), pp. 253-259.

Chen, Q., Zhu, C. & Thouas, G. A., 2012. Progress and challenges in biomaterials used for bone tissue engineering: bioactive glasses and elastomeric composites. *Progress in Biomaterials.*

Chevalier, E., Chulia, D., Pouget, C. & Viana, M., 2008. Fabrication of porous substrates: A review of processes using pore forming agents in the biomaterial field. *Journal of Pharmaceutical Sciences,* 97(3), pp. 1135-1154.

Chittibabu, V., Rao, K. S. & Rao, P. G., 2016. FACTORS AFFECTING THE MECHANICAL PROPERTIES OF COMPACT BONE. *Advances in Science and Technology Research Journal,* 10(32), p. 169–183.

Clarke, B., 2008. *Normal Bone Anatomy and Physiology.* Rochester: Clinical Journal of American Society and Nephrology.

Clement, J., Planell, J. A., Avila, G. & Martinez, S., 1999. Analysis of the structural changes of a phosphate glass during its dissolution in simulated body fluid. *Journal of Materials Science: Materials in Medicine,* 10(12), pp. 729-732.

Degrieck, J. & Paepegem, W. V., 2001. Fatigue Damage Modelling of Fibre-reinforced Composite Materials: Review. *Applied Mechanics Reviews,* 54(4), pp. 279-300.

Dhandhayuthapani, B., Yoshida, Y., Maekawa, T. & Kumar, D. S., 2011. Polymeric Scaffolds in Tissue Engineering Application: A Review. *Internatioanl Journal of Polymer Science,* Volumen 2011, p. 19.

Dorozhkin, S. V. & Epple, M., 2002. Biological and Medical Significance of Calcium Phosphates. *Angewandte International Edition Chemie,* 41(17), pp. 3130-3146.

Edward, A. y otros, 1996. Complications of Iliac Crest Bone Graft Harvesting. *Clinical Orthopaedics and Related Research,* Volumen 329, pp. 300-309.

Eqtesadi, S. y otros, 2014. Robocasting of 45S5 bioactive glass scaffolds for bone tissue engineering. *Journal of the European Ceramic Society,* 34(1), pp. 107-118.

Erasmus, E. P. y otros, 2018. In vitro Evaluation of Porous borosilicate, borophosphate and phosphate Bioactive Glasses Scaffolds fabricated using Foaming Agent for Bone Regeneration. *Scientific Reports,* 3699(8).

Filho, O. P., LaTorre, G. P. & Hench, L. L., 1996. Effect of crystallization on apatite-layer formation of bioactive glass 45%. *Journal of Biomedical Materials Research,* 30(4), pp. 509-514.

Franco, J. y otros, 2010. Direct-Write Assembly of Calcium Phosphate Scaffolds Using a Water-Based Hydrogel. *Acta Biomater,* 6(1), pp. 218-228.

Franks, K., Salih, V., Knowles, J. C. & Olsen, I., 2002. The effect of MgO on the solubility behavior and cell proliferation in a quaternary soluble phosphate based glass system. *Journal of Materials Science : Materials in Medicine,* 13(6), pp. 549-556.

Fu, Q., saiz, E., Rahaman, M. N. & Tomsia, A. P., 2011. Bioactive glass scaffolds for bone tissue engineering: state of the art and future perspectives. *Material Sciences and Engineering: C,* 31(7), pp. 1245-1256.

G., R., Venkatachalam, R. & Aravindan, S., 2012. Role of MgO on the HAp forming ability in phosphate based glasses. *Ceramics International,* 38(5), pp. 3781-3790.

Gao, H., Tan, T. & Wang, D., 2004. Effect of composition on the release kinetics of phosphate controlled release glasses in aqueous medium. *Journal of Controlled Release,* 96(1), pp. 21-28.

Gough, J. E., Christian, P., Scotchford, C. A. & Jones, I. A., 2003. Long-term craniofacial osteoblast culture on a sodium phosphate and a calcium/sodium phosphate glass. *Journal of Biomedical Materials Research - Part A,* 66(2), pp. 233-240.

Gough, J. E. y otros, 2002. Synthesis, degradation, and in vitro cell responses of sodium phosphate glasses for craniofacial bone repair. *Journal of Biomedical Materials Research,* pp. 481-489.

Graham, T., 1833. Research on the Arsenates and Phosphates and Modification of Phosphoric Acid. *Philosophical Transactions of the Royal Society ,* Volumen 123, pp. 253-284.

Gunatillake, P., Mayadunne, R. & Adhikari, R., 2006. Recent developments in biodegradable synthetic polymers. *Biotechnology Annual Review,* Volumen 12, pp. 301-347.

Gurusamy, R., Venkatachala, R. & Aravindan, S., 2012. Role of MgO on the HAp forming ability in phosphate based glasses. *Ceramics International,* 38(5), pp. 3781-3790.

Hasan, M. S. y otros, 2013. Investigating the use of coupling agents to improve the interfacial properties between a resorbable phosphate glass and polylactic acid matrix. *Journal of Biomaterials Applications,* 28(3), pp. 354-366.

Hench, L. L., 1991. Bioceramics: From Concept to Clinic. *Journal of the American Ceramics Society,* 74(7), pp. 1487-1510.

Hench, L. L., 1998. Bioceramics. *Journal of the American Ceramic Society,* 81(7), pp. 1705-1728.

Hench, L. L. & Polak, J. M., 2002. Third-Generation Biomedical Materials. *Science,* 295(5557), pp. 1014-1017.

Hench, L. L., Splinter, R. J., Allen, W. C. & Greenlee, T. K., 1971. Bonding Mechanisms at the Interface of Ceramic Prosthetic Materials. *Journal of Biomedical Materials Research,* 5(6), pp. 117-141.

Hollinger, J. O., Einhorn, T. A., Doll, B. A. & Sfeir, C., 2004. *Bone Tissue Engineering.* 1st ed. Boca Raton, London, New York, Washington D.C: CRC Press.

Huang, J. & S., B., 2014. Ceramic biomaterials for tissue engineering. En: A. R. Boccaccini & Peter X. Ma, edits. *Tissue Engineering Using Ceramics and Polymers, 2nd Edition.* s.l.:Woodhead Publishing.

Hutmacher, D. W., 2000. Scaffolds in tissue engineering bone and cartilage. *Biomaterials,* 21(24), pp. 2529-2543.

Ikada, Y., 2006. Challenges in Tissue Engineering. *Journal of The Royal Society Interface,* 3(10), pp. 589-601.

Islam, M. T. y otros, 2017. Effect of magnesium content on bioactivity of near invertphosphate-based glasses. *International Journal of Applied Glass Science,* 8(4), pp. 391-402.

Jeans, L., Gilchrist, T. & Healy, D., 2007. Peripheral nerve repair by means of a flexiblebiodegradable glass fibre wrap: A comparisonwith microsurgical epineurial repair. *Journal of Plastic, Reconstructive & Aesthetic Surgery,* Volumen 60, pp. 1302-1308.

Jian, T. y otros, 2015. Effect of Pore Size and Porosity on the Biomechanical Properties and Cytocompatibility of Porous NiTi Alloys. *PLOS ONE,* 10(6).

Jones, J. R., 2013. Review of bioactive glass: From Hench to hybrids. *Acta Biomaterialia,* 9(1), pp. 4457-4486.

Jones, J. R., Gentleman, E. & Polak, J., 2007. Bioactive Glass Scaffolds for Bone Regeneration. *Elements,* 3(6), pp. 393-399.

Kardamakis, D., Vassiliou, V. & Chow, E., 2009. *Bone Metastases-A Translational and Clinical Approach.* Patras: Springer.

Kaur, G. y otros, 2013. A review of bioactive glasses: Their structure, properties, fabrication and apatite formation. *Journal of Biomedical Materials Research,* 102(1), pp. 254-274.

Khan, Y., Yaszemski, M., Mikos, A. & Laurencin, C., 2008. Tissue Engineering of Bone: Material and Matrix Considerations. *The Journal of Bone and Joint Surgery-American,* Volumen 90, pp. 36-42.

Kokubo, T. & Takadama, H., 2006. How useful is SBF in predicting in vivo bone bioactivity?. *Biomaterials,* 27(15), pp. 2907-2915.

Kress, S., Neumann, A., Weyand, B. & Kasper, C., 2012. Stem Cell Differentiation Depending on Different Surfaces. En: C. Kasper, F. Witte & R. Pörtner, edits. *Tissue Engineering III: Cell - Surface Interactions for Tissue Culture.* s.l.:Springer, Berlin, Heidelberg, pp. 263-283.

Kumar, P., Dehiya, B. S. & Sindhu, A., 2018. Bioceramics for Hard Tissue Engineering Applications: A Review. *International Journal of Applied Engineering Research,* 13(4), pp. 2744-2752.

LEE, S., OBATA, A. & KASUGA, T., 2009. Ion release from SrO-CaO-TiO2-P2O5 glasses in Tris buffer solution. *Journal of the Ceramic Society of Japan,* 117(9), pp. 935-938.

Li, J. J., Ebied, M., Xu, J. & Zreiqat, H., 2017. Current Approaches to Bone Tissue Engineering: The Interface between Biology and Engineering. *Advanced Healthcare Materials,* 7(6).

Lindfors, N. C. y otros, 2010. A prospective randomized 14-year follow-up study of bioactive glass and autogenous bone as bone graft substitutes in benign bone tumors. *Journal of Biomedical Material Research,* 94B(1), pp. 157-164.

Liu, X., Rahaman, M. N., Hilmas, G. E. & Bal, B. S., 2013. Mechanical properties of bioactive glass (13-93) scaffolds fabricated by robotic deposition for structural bone repair. *Acta Biomater,* 9(6), pp. 7025-7034.

Lopez-Iscoa, P. y otros, 2019. Design, processing, and characterization of an optical core-bioactive clad phosphate fiber for biomedical applications. *Journal of the American Ceramic Society,* 102(11), pp. 6882-6892.

Lutolf, M. P. & Hubbell, J. A., 2005. Synthetic biomaterials as instructive extracellular microenvironments for morphogenesis in tissue engineering. *Nature Biotechnologyvolume ,* p. 47–55.

Maçon, A. L. B. y otros, 2015. A unified in vitro evaluation for apatite-forming ability of bioactive glasses and their variants. *Journal of Materials Science: Materials in Medicine,* Volumen 26, pp. 1-10.

Ma, J. y otros, 2012. Effect of MgO addition on the crystallization and in vitro bioactivity of glass ceramics in the CaO–MgO–SiO2–P2O5 system. *Ceramics International,* 38(8), pp. 6677-6684.

Ma, L. N., 2014. *Dissolution behavior of phosphate glasses,* s.l.: Missouri University of Science and Technology.

Massera, J., 2016. Bioactive Glass in Tissue Engineering: Progress and challenges. *Advances in Tissue Engineering and Regenerative Medicine,* 1(1), pp. 1-2.

Massera, J., Fagerlund, S., Hupa, L. & Hupa, M., 2012. Crystallization Mechanism of the Bioactive Glasses, 45S5 and S53P4. *Journal of American Ceramic Society,* 95(2), pp. 607-613.

Massera, J. & Hupa, L., 2014. Influence of SrO substitution for CaO on the properties of bioactive glass S53P4. *Journal of Materials Science: Materials in Medicine,* 25(3), pp. 657-668.

Massera, J. y otros, 2013. Thermal properties and surface reactivity in simulated body fluid of new strontium ion-containing phosphate glasses. *Journal of Materials Science: Materials in Medicine,* Volumen 24, pp. 1407-1416.

Massera, J. y otros, 2015. Processing and characterization of novel borophosphate glasses and fibers for medical applications. *Journal of Non-Crystalline Solids,* 425(1), pp. 52-60.

Mattioli-Belmonte, M. y otros, 2017. Pressure-activated microsyringe (PAM) fabrication of bioactive glass–poly(lactic-co-glycolic acid) composite scaffolds for bone tissue regeneration. *Journal of Tissue Engineering and Regenerative Medicine,* 11(7), pp. 1986-1997.

Mishra, A., 2019. *Phosphate Glasses and Fibers as an Alternative to Silicate Bioactive Glasses,* Tampere: Tampere University.

Mishra, A. y otros, 2017. Thermal, structural and in vitro dissolution of antimicrobial copper-doped and slow resorbable iron-doped phosphate glasses. *Journal of Materials Science,* 52(15), pp. 8957-8972.

Mishra, A., Rocherullé, J. & Massera, J., 2016. Ag-doped phosphate bioactive glasses: thermal, structural and in-vitro dissolution properties. *Biomedical Glasses,* 2(1), pp. 38-48.

Motealleh, A. y otros, 2017. Robocast 45S5 bioglass scaffolds: in vitro behavior. *Journal of Materials Science,* 52(15), p. 9179–9191.

Moustafa, Y. M. & El-Egili, K., 1998. Infrared spectra of sodium phosphate glasses. *Journal of Non-Crystalline Solids,* 240(1-3), pp. 144-153.

Moya, A. H. d. A., Aza, P. N. D., Pena, P. & Pendas, S. d. A., 1999. Bioactive glasses and glass-ceramics. *Boletin de la Sociedad Espanola de Ceramica y Vidrio ,* 46(2).

Mulligan, A. M., Wilson, M. & Knowles, J. C., 2003a. Effect of increasing silver content in phosphate-based glasses on biofilms of Streptococcus sanguis. *Journal of Biomedical Material Research,* 67A(2), pp. 401-412.

Mulligan, A. M., Wilson, M. & Knowles, J. C., 2003b. The effect of increasing copper content in phosphate-based glasses on biofilms of Streptococcus sanguis. *Biomaterials,* 24(10), pp. 1797-1807.

Nair, L. S. & Laurencin, C. T., 2007. Biodegradable polymers as biomaterials. *Progress in Polymer Science,* 32(8-9), pp. 762-798.

Neel, E. A. A. y otros, 2009. Structure and properties of strontium-doped phosphate-based glasses. *Journal of The Royal Society Interface,* 6(34), pp. 435-446.

Ojha , N., 2016. *Borosilicate Glass with Enhanced Hot Forming Properties and Conversion to Hydroxyapatite,* Tampere: Tampere University of Technology.

Pacheco, V. M.-., Hench, L. L. & Boccaccini, A. R., 2015. Bioactive glasses beyond bone and teeth: Emerging applications in contact with soft tissues. *Acta Biomaterialia,* Volumen 13, pp. 1-15.

Peltola, M. y otros, 2006. Bioactive glass S53P4 in frontal sinus obliteration: A long-term clinical experience. *Journal of the Sciences and Specialties of the Head and Neck,* Volumen 28, pp. 834-841.

Pina, S., Reis, R. L. & Oliveira, J. M., 2017. Ceramic biomaterials for tissue engineering. *Fundamentals Biomaterials: Ceramics,* Volumen 3.

POHJOLA, J., 2017. *BOROSILICATE SCAFFOLD PROCESSING FOR BONE TISSUE ENGINEERING,* Tampere: Tampere University of Technology.

Rahaman, M., 2014. Bioactive ceramics and glasses for tissue engineering. En: A. R. Boccaccini & P. X. Ma, edits. *Tissue Engineering Using Ceramics and Polymers, 2nd Edition.* s.l.:Woodhead Publishing.

Rahaman, M. N. y otros, 2011. Bioactive glass in tissue engineering. *Acta Biomaterialia,* 7(6), pp. 2355-2373.

Ratner, B. D., Hoffman, A. S., Schoen, F. J. & Lemons, J. E., 1996. *Biomaterials Science: An Introduction to Materials in Medicine.* s.l.:Academic Press.

Ray, C. S. y otros, 1996. Non-isothermal calorimetric studies of the crystallization of lithium disilicate glass. *Journal of Non-Crystalline Solids,* 204(1), pp. 1-12.

Ruiz-Aguilar, C., Aguilar-Reyes, E. A. & Olivares-Pinto, U., 2019. Microstructure and in vitro evaluation of β-TCP/ZrO2-phosphate-based bioactive glass scaffolds for bone tissue engineering. *Boletín de la Sociedad Española de Cerámica y Vidrio,* Volumen 19, p. 11.

Salernitano, E. & Migliaresi, C., 2003. Composite Materials for Biomedical Applications: A Review. *Journal of Applied Biomaterials & Biomechanic,* pp. 3-18.

Salgado, A. J., Coutinho, O. P. & Reis, R. L., 2004. Bone Tissue Engineering: State of the Art and Future Trends. *Macromolecular Bioscience,* 4(8), pp. 743-765.

Salih, V. y otros, 2000. Development of soluble glasses for biomedical use Part II: the biological response of human osteoblast cell lines to phosphate-based soluble glasses.. *Journal of materials science. Materials in medicne,* 11(10), pp. 615-20.

Salinas, A. J. & Regi, V.-R., 2013. Bioactive ceramics: from bone grafts to tissue engineering. *RSC advances,* 3(28), pp. 111116-11131.

Samavedi, S., Poindexter, L. K., Dyke, M. V. & Goldstein, A. S., 2014. Synthetic Biomaterials for Regenerative Medicine Applications. En: G. Orlando, ed. *Regenerative Medicine Applications in Organ Transplantation.* s.l.:Elsevier Science & Technology, pp. 81-99.

Sepulveda, P., Jones, J. R. & Hench, L. L., 2000. Effect of Particle Size on Bioglass Dissolution. *Key Engineering Materials,* Volumen 192-195, pp. 629-634.

Sepulveda, P., Jones, J. R. & Hench, L. L., 2002. In vitro dissolution of melt-derived 45S5 and sol-gel derived 58S bioactive glasses. *Journal of Biomedical Materials Research,* 61(2), pp. 301-311.

Shah, R. y otros, 2005. Craniofacial muscle engineering using a 3-dimensional phosphateglass fibre construct. *Biomaterials,* 26(13), pp. 1497-1505.

Shannon, R. D., 1976. Revised Effective Ionic Radii and Systematic Studies of Interatomie Distances in Halides and Chaleogenides. *Acta Crystallographica Section A,* 32(5), pp. 751-767.

Sharif, F., Rehman, I. U., Muhammad, N. & MacNeil, S., 2016. Dental materials for cleft palate repair. *Materials Science and Engineering: C,* Volumen 61, pp. 1018-1028.

Shih, P.-Y. & Shiu, H.-M., 2007. Properties and structural investigations of UV-transmitting vitreous strontium zinc metaphosphate. *Materials Chemistry and Physics,* 106(2-3), pp. 222-226.

Shih, P. Y. & Chin, T. S., 2001. Preparation of lead-free phosphate glasses with low Tg and excellent chemical durability. *Journal of Materials Science Letters,* 20(19), pp. 1811-1813.

Stevens, M. M., 2008. Biomaterials for bone tissue engineering. *materialstoday,* 11(5), pp. 18-25.

Sultana, N., 2013. *Biodegradable Polymer-Based Scaffolds for Bone Tissue Engineering.* Skudai: SpringerBriefs in Applied Sciences and Technology.

Tang, X. y otros, 2014. Polymeric Biomaterials in Tissue Engineering and Regenerative Medicine. En: S. Kumbar, C. Laurencin & M. Deng, edits. *Natural and Synthetic Biomedical Polymers.* s.l.:Elsevier Science & Technology, pp. 351-365.

Tesavibul, P. y otros, 2012. Processing of 45S5 Bioglass® by lithography-based additive manufacturing. *Materials Letters,* Volumen 74, pp. 81-84.

Tomlins, P., 2016. *Characterisation and Design of Tissue Scaffolds.* s.l.:Woodhead Publishing.

Valappil, S. P. y otros, 2007. Effect of Silver Content on the Structure and Antibacterial Activity of Silver-Doped Phosphate-Based Glasses. *Antimicrobial Agents and Chemotherapy,* 51(12), pp. 4453-4461.

Will, J., Gerhardt, L.-. C. & Boccaccini, A. R., 2012. Bioactive Glass-Based Scaffolds for Bone Tissue Engineering. En: C. Kasper, F. Witte & R. Pörtner, edits. *Tissue Engineering III: Cell - Surface Interactions for Tissue Culture.* Berlin: Springer, pp. 195-226.

Woodruff, M. A. & Hutmacher, D. W., 2010. The return of a forgotten polymer—Polycaprolactone in the 21st century. *Progress in Polymer Science,* 35(10), pp. 1217-1256.

Yeo, M. G. & Kim, G. H., 2011. Preparation and Characterization of 3D Composite Scaffolds Based on Rapid-Prototyped PCL/β-TCP Struts and Electrospun PCL Coated with Collagen and HA for Bone Regeneration. *Chemistry of Materials,* Volumen 24, pp. 903-913.

Ylänen, H. O., 2011. *Bioactive glasses: Materials, properties and applications.* s.l.:Woodhead Publishing.

Yuan, H. & Groot, K. d., 2005. *Learning from Nature How to Design New Implantable Biomaterialsis: From Biomineralization Fundamentals to Biomimetic Materials and Processing Routes.* s.l., Springer, Dordrecht.